Eur. Phys. J. C (2025) 85:413
https://doi.org/10.1140/epjc/s10052-025-14143-8

THE EUROPEAN PHYSICAL JOURNAL C

Regular Article - Theoretical Physics

Investigating the effects of gravitational lensing by Hu-Sawicki $f(R)$ gravity black holes

Gayatri Mohan[1,a], **Nashiba Parbin**[2,3,b], **Umananda Dev Goswami**[1,c]

[1] Department of Physics, Dibrugarh University, Dibrugarh, Assam 786004, India
[2] Department of Physics, AMC Engineering College, Bangalore, Karnataka 560083, India
[3] Visvesvaraya Technological University (VTU), Belagavi, Karnataka 590018, India

Received: 8 December 2024 / Accepted: 30 March 2025

Abstract In this work, gravitational lensing in the weak and strong field limits is investigated for black hole spacetime within the framework of Hu–Sawicki $f(R)$ gravity. We employ the Ishihara et al. approach for weak lensing and adopt Bozza's method for strong lensing to explore the impact of Hu–Sawicki model parameters on lensing phenomenon. The deflection angles are computed and analyzed in both the field limits. Our investigation in the weak as well as the strong lensing reveals that in the case of Hu–Sawicki black holes, photons exhibit divergence at smaller impact parameters for different values of the model parameters compared to the Schwarzschild scenario and the photon experiences negative deflection angle when impact parameter moves towards the larger impact parameter values. Additionally, by calculating strong lensing coefficients we study their behavior with model parameters. The strong lensing key observables associated with the lensing effect viz. the angular position ϑ_∞, angular separation s and relative magnification r_{mag} are estimated numerically by extending the analysis to supermassive black holes SgrA* and M87* and analyzed their behavior concerning the parameters for each black hole. The analysis shows that SgrA* demonstrates larger values of ϑ_∞ and s relative to M87*.

1 Introduction

The predictions of black holes (BHs) and gravitational waves (GWs) are the two most incredible and noteworthy achievements of Einstein's theory of General Relativity (GR), published in 1915 [1,2]. The historic triumph of the Event Horizon Telescope (EHT) in capturing the first photographs of the supermassive BHs M87* [3] and SgrA* [4] have unfurled new aspects for studying BHs thereby fetching more attention as one of the active areas in modern astrophysics. In essence, the study of the optical features of BHs has prompted considerable interest amongst the scientific population. This dynamic is persistently advancing with enhanced technologies and the accumulation of fresh data. In passing it needs to be mentioned that the detection of GWs by the LIGO detector system in 2015 [5,6] is another significant milestone of GR on its avenue of success, which unfolded different ways of looking into the Universe.

EHT's BH images and detection of GWs by LIGO have successfully corroborated predictions of Einstein's GR, simultaneously raising queries on the consequential challenges faced by it, which include deciphering the expansion history of the Universe [7,8], the observed rotational dynamics of the galaxies [9–13], the need for exotic stuff such as dark matter and dark energy [14–16], existence of spacetime singularities within BHs [17], the large scale structure [18], etc. These led to an extensive investigation of different theories of gravity beyond the GR framework, known as modified theories of gravity (MTGs) [19,20], where higher curvature terms or extra fields are incorporated in the Einstein–Hilbert (EH) action. In recent times, a plethora of MTGs [21–29] have been introduced which impart richer frameworks to comprehend gravity in a better way. $f(R)$ theory of gravity [30,31] is one of the most straightforward extensions that lays out a constructive way to interpret the basic principles and limitations behind the modification of GR. It has been under detailed investigation over the years [32–40] and is categorized under those theories that encompass higher-order curvature invariants. Currently, a few models of $f(R)$ gravity have been proposed. The Starobinsky model [41], the Hu–

[a] e-mail: gayatrimohan704@gmail.com
[b] e-mail: nashibaparbin91@gmail.com
[c] e-mail: umananda@dibru.ac.in (corresponding author)

Published online: 13 April 2025

Sawicki model [42], the Tsujikawa model [43], and another recently introduced model [44] are a few of the known viable $f(R)$ gravity models. In literature, these models have been rigorously studied in various aspects such as unraveling the mystery of dark matter [35,45], puzzles of the early Universe [46], cosmological and astrophysical consequences of these models [47,48], and so on.

In 1919, Arthur Eddington, Frank Dyson and Charles Davidson detected the deflection in the path of light emerging from stars in the Hyades cluster, around the sun during a solar eclipse [49]. This groundbreaking observation served as the first experimental proof of Einstein's GR and thus emerged the beautiful phenomenon of gravitational lensing [50,51]. Extensively studied in cosmology and astronomy [52–55], lensing occurs as light from a distant source gets deviated in the vicinity of massive objects, such as BHs, galaxy clusters, etc. The deflection angle allows us to study the optical properties of such massive objects. BHs exhibit exceptional laboratories to explore strong gravitational effects. Implementing the magnificent phenomenon of gravitational lensing on BHs, it is feasible to classify a variety of BH models [56–62] and also to test different theories of gravity [62–69]. Gravitational lensing can also act as a robust astrophysical tool for the study of the gravitational field of massive objects as well as for uncovering the mystery of dark matter [70–72].

When numerous photons reach the vicinity of BHs, the effects of gravitational lensing can be observed which contribute towards the formation of distinct features of the BH such as its shadow, relativistic images at the event horizon, and a photon ring. To figure out these gravitational field features of the BH from the observational as well as theoretical standpoint, a pivotal role is portrayed by the study of the null geodesics around the BH. In the strong field limit, the foundational work contributed by Darwin [73] to interpret the lensing effects marked the dawn of research in this area. Such studies in the strong field limit have gained considerable recognition in recent years as more information on BHs can be extracted from the same [74–86]. Virbhadra and Ellis explored the Schwarzschild BH to investigate various aspects of gravitational lensing. They first formulated the lens equation in the strong field domain [87]. Next, they analyzed the behavior of relativistic images for a Schwarzschild BH [88–90]. They further explored the lensing by naked singularities [91]. Many studies also involved the analysis of time delays caused due to gravitational lensing in the strong field limit [92–98]. Studies concerning the weak field limit come into play when we consider the photons to be at a significant distance from the BH. At this point, the strong field limit does not remain relevant. In 2008, Gibbons and Werner ventured on the path to study the gravitational lensing features in the weak field limit [99] and proposed an alternative approach. They implemented the Gauss–Bonnet Theorem (GBT) [100,101] to derive the deflection of light in the weak gravitational field of a static spherically symmetric spacetime. A number of articles have revealed that this approach can be utilized to deduce the deflection angle for various BH spacetimes [102–111]. Subsequently, Werner developed their analysis of axially symmetric spacetimes implementing Finsler geometry [112,113], although this approach is found to be a bit challenging. A few years later, in 2016, Ishihara and his co-workers developed the Gibbons-Werner approach further while considering finite distances [114]. Refs. [98,106,115–117] report the use of this extension for stationary spacetimes. Furthermore, for non-asymptotically flat BHs, the use of this extended approach is reported in Refs. [62,64,118–121]. In the last decade, studies of gravitational lensing around naked singularities [122–124], wormholes [125–127] and other exotic objects [128,129] have also increased along with the study of lensing in spacetimes surrounded by dark matter [130,131].

Motivated by the factors presented above, our research tends to investigate the lensing features of a BH within the framework of Hu–Sawicki $f(R)$ gravity model [132]. In this theory, the BH spacetime has been recently deduced [132] which makes it more intriguing to explore the gravitational bending elements in the weak as well as strong field limits. For the weak field lensing, the Ishihara et al. approach is employed to analyze the effects of the Hu–Sawicki model parameters on the bending angle of light as it reaches the vicinity of such a BH. Next, the strong field lensing is studied by implementing the methodologies forwarded by Bozza [74] and the effect of the model parameter on the lensing observables is also investigated.

The remaining paper is organized in the following pattern. In Sect. 2, we give a brief explanation of the framework that is to be used for the proposed research. In Sect. 3, we deduce the deflection angle for the weak field limit. In Sect. 4, the gravitational bending angle of light is derived in the strong field limit of the BH spacetime. In addition, in this section, the lensing observables are also computed and analyzed in the $f(R)$ gravity framework. In Sect. 5, we summarize and conclude the findings of our research.

2 Black holes in Hu–Sawicki $f(R)$ gravity theory

Modifying Einstein's GR is an intricate and challenging piece of work. As mentioned earlier, $f(R)$ gravity theory is one of the simplest modifications of GR and hence, is considered frequently for various astrophysical and cosmological studies. One compelling advantage of this theory is that it can avoid the Oströgradsky instability [133]. Indeed, Oströgradsky instability is a fundamental issue that arises in field theories when equations of motion involve higher-order derivatives. This instability gives rise to a ghost degree of freedom and results in a system with unbounded Hamiltonians,

i.e. the energy can become arbitrarily negative, causing runaway solutions and making the theory physically inconsistent. The fundamental cause of this instability lies in the Hamiltonian formulation of higher-derivative theories. It is a consequence of Oströgradsky's theorem, which states that a non-degenerate Lagrangian containing higher than second-order time derivatives leads to a Hamiltonian that is not bounded from below [134].

It is well known that in order to deduce the field equations of $f(R)$ gravity, the first step is to rewrite the EH action by replacing the Ricci scalar R with a function of R, usually designated as $f(R)$. The generic action that defines the $f(R)$ gravity theory is specified as [30]

$$S = \frac{1}{2\kappa}\int d^4x\sqrt{-g}\,f(R) + S_m, \tag{1}$$

where $\kappa = 8\pi G c^{-4}$ and the action of matter is denoted by S_m. Varying the above action with respect to the metric $g_{\mu\nu}$, we arrive at the field equations for $f(R)$ gravity as given by

$$F R_{\mu\nu} - \frac{1}{2}f(R)g_{\mu\nu} - (\nabla_\mu\nabla_\nu - g_{\mu\nu}\Box)F = \kappa T_{\mu\nu}, \tag{2}$$

where F is obtained by differentiating $f(R)$ with respect to R, and $\Box = \nabla_\alpha\nabla^\alpha$. The energy momentum tensor $T_{\mu\nu}$ is given as

$$T_{\mu\nu} = \frac{-2}{\sqrt{-g}}\frac{\delta(\sqrt{-g}S_m)}{\delta g_{\mu\nu}}. \tag{3}$$

Trace of Eq. (2) can be obtained as

$$f(R) = \frac{1}{2}\big[3\Box F + FR - \kappa T\big]. \tag{4}$$

This equation contains fourth-order derivatives of the metric through $\Box F$. It is a dynamical equation that suggests F as an additional propagating degree of freedom in the theory. This extra degree of freedom accounts for the deviations from GR.

In Ref. [132], the authors have deduced a BH spacetime in the Hu–Sawicki model [42] of $f(R)$ gravity. This model represents one of the viable functional forms of the $f(R)$ gravity theory which is found to be consistent observationally in cosmological scales [135,136]. In 2007, Wayne Hu and Ignacy Sawicki came up with this model to interpret the present accelerating Universe excluding the cosmological constant. One of its interesting traits is that it is able to meet the requirements of the solar system tests thereby being valid in the local scales too. Presently, numerous research works are employing the Hu–Sawicki model to investigate diverse aspects of cosmology and astrophysics [137–140]. The model is presented as

$$f(R) = -m^2\frac{c_1\left(\frac{R}{m^2}\right)^n}{c_2\left(\frac{R}{m^2}\right)^n + 1}, \tag{5}$$

where $n > 0$, c_1 and c_2 are dimensionless model parameters and m is another parameter, the square of which depicts the mass (energy) scale [42]. The functional form of the Hu–Sawicki $f(R)$ model given by Eq. (5) is such that it fulfills certain desirable observational criteria. Without invoking a true cosmological constant, it can drive late-time cosmic acceleration with an expansion history that closely resembles the ΛCDM model [141,142]. It satisfies an asymptotic behavior similar to the ΛCDM model in the large curvature region. The model, at $R \to \infty$ yields $f(R) =$ constant, thus mimicking the ΛCDM model in the large curvature region. Moreover, at $R \to 0$ it gives $f(R) = 0$ [44]. It is important to emphasize that, similar to other viable $f(R)$ models, the Hu–Sawicki $f(R)$ function is also designed to meet the stability requirement $d^2 f(R)/dR^2 > 0$ [42,143,144]. Furthermore, its field equations can be rewritten in a second-order form, allowing the theory to be reformulated as a second-order scalar-tensor theory. This is achieved by identifying the extra degree of freedom F as a scalar field ϕ [35]. It ensures that the theory remains free from the Oströgradsky instability. Additionally, the explicit dependence of F on curvature R dynamically couples the scalar field ϕ to R. Consequently, variations of curvature caused by matter distributions directly impact the scalar field.

Now, the considered metric ansatz is given by

$$ds^2 = -A(r)dt^2 + B(r)dr^2 + r^2(d\theta^2 + \sin^2\theta\, d\phi^2). \tag{6}$$

The metric coefficients of the spacetime that are deduced for the Hu–Sawicki $f(R)$ gravity model in the form [132]:

$$\begin{aligned} A(r) = \frac{1}{B(r)} &= 1 - \frac{2M}{r} + \frac{m^2}{12}\left(\frac{n-2}{2c_2}\right)^{1/n} r^2 \\ &= 1 - \frac{2M}{r} + \lambda\, r^2, \end{aligned} \tag{7}$$

where M is the BH mass parameter and $\lambda = m^2/12\,((n-2)/2c_2)^{1/n}$. It can be seen from the aforementioned relation that the BH spacetime does not depend on the model parameter c_1. Hence, in our work, we shall analyze the effect of the parameters c_2 and m on the deflection angle of the BH spacetime in the weak as well as strong field regime. Also, we shall investigate the effect of these parameters on the lensing observables in the strong field limit.

However, before proceeding to the proposed analyses, for completeness, it would be appropriate to make a few comments on the considered BH solution. It is seen from

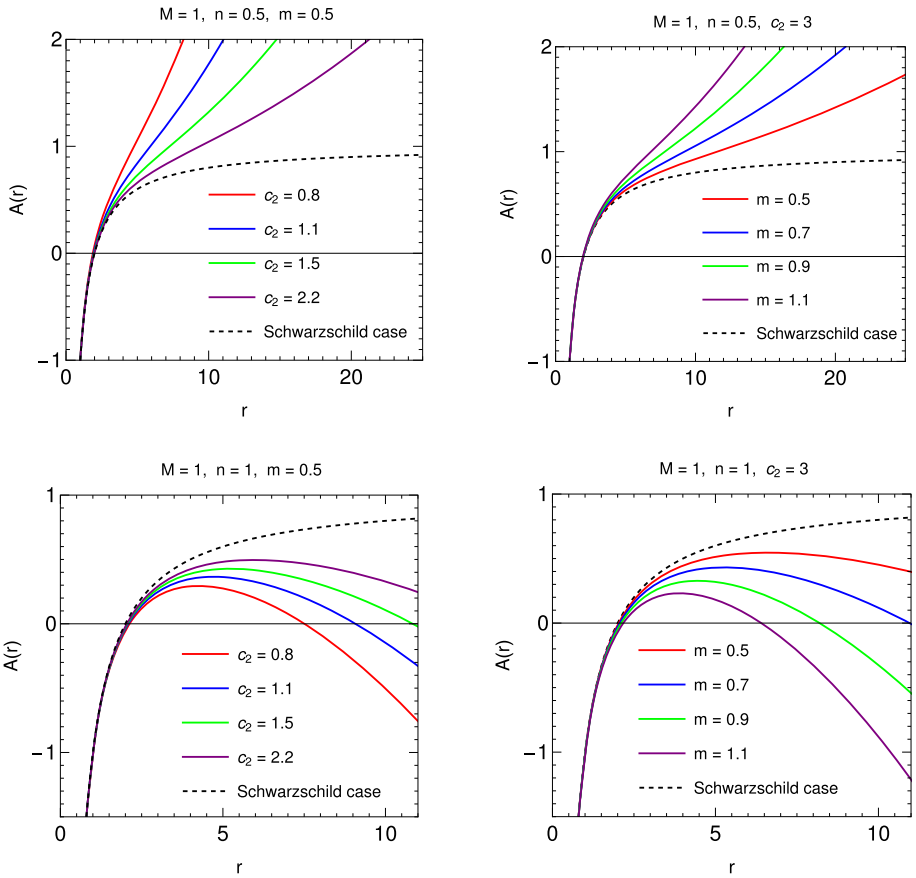

Fig. 1 The behavior of the metric function $A(r)$ with respect to radial distance r for Hu–Sawicki model BHs with different values of model parameters. The left two plots illustrate the behavior of the function as c_2 changes for $n = 0.5$ and $n = 1$ respectively. The right two plots display the behavior of the function with variation of m for the same values of the parameter n

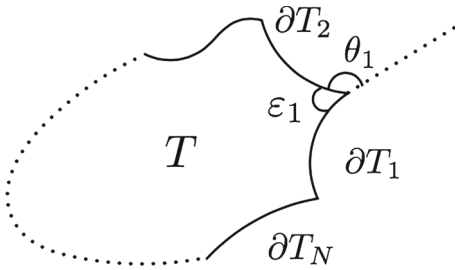

Fig. 2 Schematic representation for the GBT [114]. The inner angle is ε_a and the jump angle is θ_a $(a = 1, 2, \ldots, N)$

Eq. (7) that as λ equals to zero, this solution reduces to the Schwarzschild BH solution. The horizons of the BHs represented by Eq. (7) are the positive real roots of equation $A(r) = 0$. Depending on different sets of parameter values the solution reveals that the BHs exhibit either a single, well-defined event horizon analogous to the Schwarzschild BH or two distinct horizons as shown in Fig. 1. It is observed that in the presence of two horizons, the outer horizon moves away from the inner one when c_2 increases whereas it approaches the inner horizon as m increases. Beyond a specific higher value of the parameter m and a sufficiently lower value of c_2, the BHs become a horizonless singularity for the given values of other parameters.

3 Gravitational bending of light in the weak field limit

A key parameter in probing the captivating phenomenon of gravitational lensing is the bending angle of light. In the weak field limit of deflection of light, the point of closest approach of photons traveling from a distant source is found to be far away from the lensing mass which in our case is the mass of the BH. In this section, the deflection angle shall be deduced in the weak field limit of the Hu–Sawicki $f(R)$ gravity BH spacetime (6). We tend to analyze the effect of the model parameters on the angle of bending of light as it approaches the weak gravitational field of the BH. With that in mind, we follow the Ishihara et al. approach for asymptotically non-flat spacetimes presented in Ref. [114]. In this approach, the GBT is employed to compute the angle of bending of light. Several formulations of GBT exist and among them, the simplest one theorizes that the total Gaussian curvature surrounded by an enclosed triangle can be denoted in terms of the total geodesic curvature of the boundary and the jump angles formed at the corners. This theorem can be comprehended by following the illustration shown in Fig. 2. An orientable surface T is portrayed in two dimensions, whose boundaries are differentiable curves. These curves are represented as ∂T_a $(a = 1, 2, \ldots, N)$ with θ_a as the jump angles formed between the curves. Consequently, the GBT can be

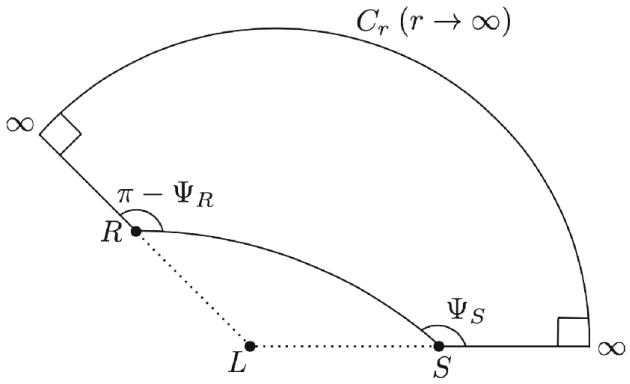

Fig. 3 Illustrative description for the quadrilateral $\overset{\infty}{R}\square\overset{\infty}{S}$ enclosed in a curved space [120]

mathematically defined as [100]

$$\int\int_T \mathcal{K} dS + \sum_{a=1}^{N} \int_{\partial T_a} \kappa_g dl + \sum_{a=1}^{N} \theta_a = 2\pi, \tag{8}$$

where $\mathcal{K}$ denotes the Gaussian curvature of the surface T, κ_g is the geodesic curvature of the boundaries ∂T_a with an infinitesimal line element dl along the boundary. The sign of dl is chosen in such a way that it is in accordance with the orientation of the surface following $dl > 0$ for prograde motion and $dl < 0$ for retrograde motion of photons.

In Fig. 3, the BH is portrayed as a lens (L) with the source (S) and the receiver (R) located at a finite distance from L. In view of the equatorial plane ($theta = \pi/2$), the deflection angle of light approaching from the source can be presented as [114,115]

$$\hat{\alpha} = \Psi_R - \Psi_S + \phi_{RS}, \tag{9}$$

where Ψ_R and Ψ_S exhibit the angles of light approximated with respect to L at the positions of S and R respectively. ϕ_{RS} is the separation angle between R and S, and is signified by $\phi_{RS} = \phi_R - \phi_S$ where ϕ_R and ϕ_S are the longitudes of R and S respectively.

The null condition which signifies $ds^2 = 0$ is followed by the light rays. Consequently, the BH metric can be recast as

$$dt^2 = \gamma_{ij} dx^i dx^j = \frac{1}{A(r)^2} dr^2 + \frac{r^2}{A(r)} d\Omega^2, \tag{10}$$

where γ_{ij} is usually indicated as the optical metric and $d\Omega^2 = d\theta^2 + \sin^2\theta\, d\phi^2$. It describes a 3D Riemannian space represented by $\mathcal{M}^{(3)}$. In this manifold, a ray of light is interpreted as a spatial curve. The non-vanishing components of the optical metric are

$$\gamma_{rr} = \frac{1}{A(r)^2}, \quad \gamma_{\phi\phi} = \frac{r^2}{A(r)}. \tag{11}$$

Another parameter of paramount importance in the study of the bending of light is the impact parameter. It is typically defined as the ratio of the angular momentum ($\mathcal{L}$) and the energy ($\mathcal{E}$) of photons. In the equatorial plane of spacetime, $\mathcal{L}$ and $\mathcal{E}$ are the constants of motion and for the spacetime (6), these can be represented as $\mathcal{E} = A(r)\,\dot{t}$ and $\mathcal{L} = r^2\,\dot{\phi}$, where the over dot depicts the derivative with respect to the affine parameter τ along the path of the light ray. Hence, the impact parameter is given as

$$\zeta \equiv \frac{\mathcal{L}}{\mathcal{E}} = \frac{r^2}{A(r)} \frac{d\phi}{dt}. \tag{12}$$

The unit radial vector along the radial direction from the center of the lens and the unit angular vector across the angular path are respectively obtained as $e_{rad} = (A(r), 0)$ and $e_{ang} = (0, A(r)/r)$. Moreover, the components of the unit tangent vector $\boldsymbol{K} \equiv d\boldsymbol{x}/dt$ along the path of the light ray are obtained as [114]

$$(K^r, K^\phi) = \frac{\zeta A(r)}{r^2} \left(\frac{dr}{d\phi}, 1\right). \tag{13}$$

The term $dr/d\phi$ in the above expression results in the orbit equation as

$$\left(\frac{dr}{d\phi}\right)^2 = -r^2 A(r) + \frac{r^4}{\zeta^2}. \tag{14}$$

Now, if Ψ is assumed to be the angle of the light ray estimated from the radial direction, then we have

$$\cos\Psi = \frac{\zeta}{r^2} \frac{dr}{d\phi}, \tag{15}$$

which leads to,

$$\sin\Psi = \frac{\zeta\sqrt{A(r)}}{r}. \tag{16}$$

Again, considering a new variable $u = 1/r$, we can recast Eq. (14) as

$$\left(\frac{du}{d\phi}\right)^2 = F(u), \tag{17}$$

where the function $F(u)$ is obtained as $F(u) = -u^2\,A(u) + 1/\zeta^2$.

At this stage, it needs to be pointed out that the quadrilateral $\overset{\infty}{R}\square\overset{\infty}{S}$ portrayed in Fig. 3 is enclosed within the space $\mathcal{M}^{(3)}$. This quadrilateral $\overset{\infty}{R}\square\overset{\infty}{S}$ comprises of light rays behaving as spatial curves with two outgoing radial lines from receiver and source, along with a circular arc fragment C_r with the coordinate radius r_C ($r_C \to \infty$). It is

clearly observed from Fig. 3 that within the asymptotically flat Minkowskian spacetime, $\kappa_g \to 1/r_C$ and $dl \to r_C\, d\phi$ as $r_C \to \infty$ [99]. Accordingly, we can present the bending angle of light in the domain $\overset{\infty}{R}\square\overset{\infty}{S}$ as

$$\hat{\alpha} = \Psi_R - \Psi_S + \phi_{RS} = -\int\int_{\overset{\infty}{R}\square\overset{\infty}{S}} \mathcal{K}\, dS. \tag{18}$$

Integrating Eq. (17), the separation angle ϕ_{RS} can be obtained as

$$\phi_{RS} = 2\int_0^{u_0} \frac{du}{\sqrt{F(u)}}, \tag{19}$$

where u_0 denotes the inverse of the distance of the closest approach. Corresponding to the Ishihara *et al.* approach followed in this work, if S and R positions are considered to be at finite distances from the BH, the gravitational deflection angle can be represented as

$$\hat{\alpha} = \Psi_R - \Psi_S + \int_{u_R}^{u_0} \frac{du}{\sqrt{F(u)}} + \int_{u_S}^{u_0} \frac{du}{\sqrt{F(u)}}. \tag{20}$$

Now, applying Eq. (16) to the BH metric (6), we arrive at

$$\begin{aligned}
\Psi_R - \Psi_S &= \arcsin(\zeta u_R) + \arcsin(\zeta u_s) - \pi + \zeta M \\
&\times \left(\frac{u_R^2}{\sqrt{1-\zeta^2u_R^2}} + \frac{u_S^2}{\sqrt{1-\zeta^2u_S^2}}\right) \\
&+ \frac{2^{-2-\frac{1}{n}}}{3}\zeta^3 m^2 M \left(\frac{u_R^2}{(1-\zeta^2u_R^2)^{3/2}} + \frac{u_S^2}{(1-\zeta^2u_S^2)^{3/2}}\right) \\
&+ \frac{\zeta M^2}{2}\left(\frac{u_R^3}{(1-\zeta^2u_R^2)^{3/2}} + \frac{u_S^3}{(1-\zeta^2u_S^2)^{3/2}}\right) \\
&- \frac{2^{-3-\frac{1}{n}}}{3}\zeta m^2 M \left(\frac{1}{(1-\zeta^2u_R^2)^{3/2}} + \frac{1}{(1-\zeta^2u_S^2)^{3/2}}\right) \\
&- 2^{-4-\frac{1}{n}}\zeta m^2 M^2 \left(\frac{n-2}{c_2}\right)^{1/n}\left(\frac{u_R}{(1-\zeta^2u_R^2)^{5/2}}\right. \\
&\left.+\frac{u_S}{(1-\zeta^2u_S^2)^{5/2}}\right) + \frac{2^{-1-\frac{1}{n}}}{3}\zeta^3 m^2 M^2 \left(\frac{n-2}{c_2}\right)^{1/n} \\
&\times \left(\frac{u_R^3}{(1-\zeta^2u_R^2)^{5/2}} + \frac{u_S^3}{(1-\zeta^2u_S^2)^{5/2}}\right) \\
&- \frac{2^{-3-\frac{1}{n}}}{3}\zeta m^2 \left(\frac{n-2}{c^2}\right)^{1/n}\left(\frac{u_R^{-1}}{\sqrt{1-\zeta^2u_R^2}} + \frac{u_S^{-1}}{\sqrt{1-\zeta^2u_S^2}}\right).
\end{aligned} \tag{21}$$

It is evident that this expression tends to become divergent at $u_R \to 0$ and $u_S \to 0$ due to the fact that the spacetime under consideration is asymptotically non-flat. Thus, this series Eq. (21) must be employed only within a certain limit of the finite radius of convergence.

Next, the angle ϕ_{RS} is computed for the BH spacetime (6) as

$$\begin{aligned}
\phi_{RS} &= \pi - \arcsin(\eta u_R) - \arcsin(\eta u_S) \\
&+ \left[\frac{15M^2}{4\zeta^2} + 5\times 2^{-4-\frac{1}{n}} m^2 M^2 \left(\frac{n-2}{c_2}\right)^{1/n}\right] \\
&\times (\pi - \arcsin(\eta u_R) \\
&- \arcsin(\eta u_S)) - \frac{2^{-3-\frac{1}{n}}}{3}\zeta^3 m^2 \left(\frac{n-2}{c_2}\right)^{1/n} \\
&\times \left(\frac{u_R}{\sqrt{1-\zeta^2u_R^2}} + \frac{u_S}{\sqrt{1-\zeta^2u_S^2}}\right) \\
&+ \left[\frac{2M}{\zeta} - \frac{2^{-2-\frac{1}{n}}}{3}\zeta m^2 M \left(\frac{n-2}{c_2}\right)^{1/n}\right] \\
&\times \left(\frac{1}{(1-\zeta^2u_R^2)^{3/2}} + \frac{1}{(1-\zeta^2u_S^2)^{3/2}}\right) \\
&- \left[3\zeta M - 2^{-2-\frac{1}{n}}\zeta^3 m^2 M \left(\frac{n-2}{c_2}\right)^{1/n}\right] \\
&\times \left(\frac{u_R^2}{(1-\zeta^2u_R^2)^{3/2}} + \frac{u_S^2}{(1-\zeta^2u_S^2)^{3/2}}\right) \\
&+ \left[\frac{15M^2}{4\zeta} + 5\times 2^{-4-\frac{1}{n}}\zeta m^2 M^2 \left(\frac{n-2}{c_2}\right)^{1/n}\right] \\
&\times \left(\frac{u_R^2}{(1-\zeta^2u_R^2)^{5/2}} + \frac{u_S^2}{(1-\zeta^2u_S^2)^{5/2}}\right) \\
&- \left[\frac{35\zeta M^2}{4} + \frac{35\times 2^{-4-\frac{1}{n}}}{3}\zeta^3 m^2 M^2 \left(\frac{n-2}{c_2}\right)^{1/n}\right] \\
&\times \left(\frac{u_R^3}{(1-\zeta^2u_R^2)^{5/2}} + \frac{u_S^3}{(1-\zeta^2u_S^2)^{5/2}}\right).
\end{aligned} \tag{22}$$

Finally, by combining Eqs. (21) and (22), we arrive at the bending angle of light in the gravitational field of the Hu–Sawicki $f(R)$ gravity BH under the study and is presented as

$$\hat{\alpha} = \left[\frac{15M^2}{4\zeta^2} + 5\times 2^{-4-\frac{1}{n}} m^2 M^2 \left(\frac{n-2}{c_2}\right)^{1/n}\right] \times (\pi - \arcsin(\eta u_R) - \arcsin(\eta u_S)) - 2^{-2-\frac{1}{n}}\zeta^3 m^2 \left(\frac{n-2}{c_2}\right)^{1/n}\left(\frac{u_R}{\sqrt{1-\zeta^2u_R^2}} + \frac{u_S}{\sqrt{1-\zeta^2u_S^2}}\right) + \zeta M\left(\frac{u_R^2}{\sqrt{1-\zeta^2u_R^2}} + \frac{u_S^2}{\sqrt{1-\zeta^2u_S^2}}\right) + \left[3\times 2^{-3-\frac{1}{n}}\zeta^3 m^2 M\left(\frac{n-2}{c_2}\right)^{1/n} - 3\zeta M\right] \times \left(\frac{u_R^2}{(1-\zeta^2u_R^2)^{3/2}} + \frac{u_S^2}{(1-\zeta^2u_S^2)^{3/2}}\right) + \frac{\zeta M^2}{2}\left(\frac{u_R^3}{(1-\zeta^2u_R^2)^{3/2}} + \frac{u_S^3}{(1-\zeta^2u_S^2)^{3/2}}\right) + \left[\frac{2M}{\zeta} - 2^{-3-\frac{1}{n}}\zeta m^2 M\left(\frac{n-2}{c_2}\right)^{1/n}\right] \times \left(\frac{1}{(1-\zeta^2u_R^2)^{3/2}} + \frac{1}{(1-\zeta^2u_S^2)^{3/2}}\right) - 2^{-4-\frac{1}{n}}\zeta m^2 M\left(\frac{n-2}{c_2}\right)^{1/n} \times \left(\frac{u_R}{(1-\zeta^2u_R^2)^{5/2}} + \frac{u_S}{(1-\zeta^2u_S^2)^{5/2}}\right) + \left[\frac{15M^2}{4\zeta} + 5\times 2^{-4-\frac{1}{n}}\zeta m^2 M^2\left(\frac{n-2}{c_2}\right)^{1/n}\right] \times \left(\frac{u_R^2}{(1-\zeta^2u_R^2)^{5/2}} + \frac{u_S^2}{(1-\zeta^2u_S^2)^{5/2}}\right) + \left[-\frac{35\zeta M^2}{4} + 9\times 2^{-4-\frac{1}{n}}\zeta^3 m^2 M^2\left(\frac{n-2}{c_2}\right)^{1/n}\right] \times \left(\frac{u_R^3}{(1-\zeta^2u_R^2)^{5/2}} + \frac{u_S^3}{(1-\zeta^2u_S^2)^{5/2}}\right) - \frac{2^{-3-\frac{1}{n}}}{3}\zeta m^2\left(\frac{n-2}{c_2}\right)^{1/n}\left(\frac{u_R^{-1}}{\sqrt{1-\zeta^2u_R^2}} + \frac{u_S^{-1}}{\sqrt{1-\zeta^2u_S^2}}\right). \tag{23}$$

As a consequence of a few terms present in Eq. (21), the above expression also becomes divergent in the far distance limit ($u_R \to 0, u_S \to 0$). The reason behind this was stated earlier as that the spacetime under study is asymptotically non-flat, analogous to the Kottler spacetime [145] employed by Ishihara et al. [114]. In their work, Ishihara et al. discussed this issue of the divergence of the deflection angle and stated that such an issue is not of much concern as the limit $u_R \to 0$, $u_S \to 0$ is not applicable for astronomical observations. Also, due to the analogy between the BH metric (7) and the Kottler spacetime mentioned above, the deflection angle derived in our study appears to coincide with that derived in Ref. [114]. However, for both instances, the effective cosmological constant will affect the deflection angle in significantly different manners. The reason behind this is that in our case, the effective cosmological constant depends on two important Hu–Sawicki model parameters m and c_2. Furthermore, the effect of the Hu–Sawicki model parameter on the deflection angle $\hat{\alpha}$ can be evidently analyzed from the aforementioned equation. However, if the model parameters are to vanish, i.e. $n = m = c_2 = 0$, it would result in

$$\hat{\alpha} = \frac{15M^2}{4\zeta^2}(\pi - \arcsin(\eta u_R) - \arcsin(\eta u_S)) + \zeta M\left(\frac{u_R^2}{\sqrt{1-\zeta^2u_R^2}} + \frac{u_S^2}{\sqrt{1-\zeta^2u_S^2}}\right) - 3\zeta M\left(\frac{u_R^2}{(1-\zeta^2u_R^2)^{3/2}} + \frac{u_S^2}{(1-\zeta^2u_S^2)^{3/2}}\right) + \frac{\zeta M^2}{2}\left(\frac{u_R^3}{(1-\zeta^2u_R^2)^{3/2}} + \frac{u_S^3}{(1-\zeta^2u_S^2)^{3/2}}\right) + \frac{2M}{\zeta}\left(\frac{1}{(1-\zeta^2u_R^2)^{3/2}} + \frac{1}{(1-\zeta^2u_S^2)^{3/2}}\right) + \frac{15M^2}{4\zeta}\left(\frac{u_R^2}{(1-\zeta^2u_R^2)^{5/2}} + \frac{u_S^2}{(1-\zeta^2u_S^2)^{5/2}}\right) - \frac{35\zeta M^2}{4}\left(\frac{u_R^3}{(1-\zeta^2u_R^2)^{5/2}} + \frac{u_S^3}{(1-\zeta^2u_S^2)^{5/2}}\right). \tag{24}$$

which in the far distance limit ($u_R \to 0, u_S \to 0$) yields the bending angle of light for a Schwarzschild BH and is deduced as

$$\hat{\alpha} \simeq \frac{4M}{\zeta} + \frac{15M^2\pi}{4\zeta^2} \tag{25}$$

In Fig. 4, we portray the deflection angle formed as a result of the bending of light in the weak gravitational field of the Hu–Sawicki $f(R)$ gravity BH as a function of the impact parameter and analyze the effects of the model parameters m and c_2 on the deflection angle. In our analysis, we have taken $u_R = u_S = 0.5/\zeta$. It is evident from the two graphical depictions displayed in Fig. 4 that for each plot the computed results are compared with that of the Schwarzschild case. We can refer from each representation that for both cases, the deflection angle decreases with an increase in the impact parameter analogous to the Schwarzschild case up to

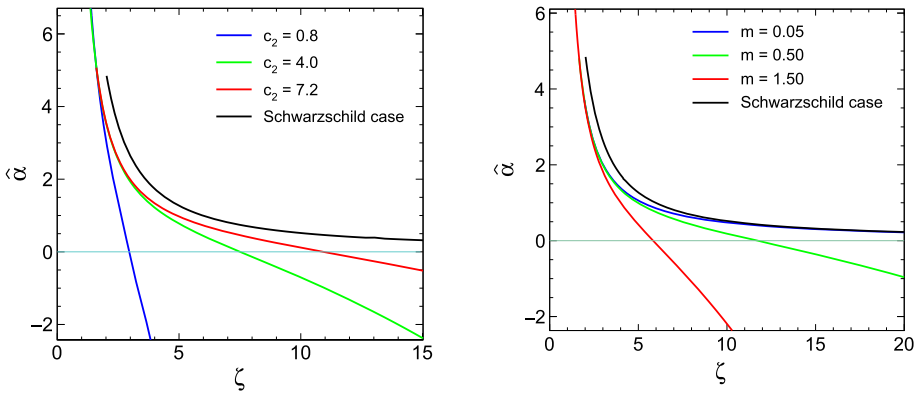

Fig. 4 Deflection angle as a function of the impact parameter ζ for different values of the Hu–Sawicki model parameters c_2 and m with $M = 1$, and $n = 0.5$

a certain limit and then unlike the Schwarzschild case, the deflection angle continues to decrease with increasing impact parameter and becomes negative. In the first illustration, we have considered three different values of $c_2 = 0.8, 4.0, 7.2$ and compared the deflection angle for these values with the Schwarzschild case. It is observed from the figure that as the value of c_2 increases, the deflection angle tries to mimic the Schwarzschild behaviour. However, when observed for much higher impact parameters, the deflection angle is still found to stay on the negative end. For the case of different m values $m = 0.05, 0.5, 1.50$, it can be seen that for lower m values, the deflection angle slowly moves towards the positive end for higher impact parameters. For $m = 0.05$, the deflection angle is seen to overlap with the Schwarzschild case for higher impact parameter values. Thus, it can be said that for smaller m values, the Schwazschild behaviour can be recovered from the Hu–Sawicki $f(R)$ gravity BH beyond certain values of the impact parameter. For the negative deflection angle, it can be remarked that for high values of the impact parameter, the photons suffer repulsion by the gravitational field of the BH. Such a negative deflection angle presents an idea regarding the nature of the gravitational field of the BH. A number of research works [63,119,146,147] have also arrived at a negative deflection angle.

4 Gravitational lensing in the strong field limit

In the strong field gravitational lensing, a photon from a distant source approaches very close to a massive object such as a BH and experiences an intense gravitational field of the object. Consequently, it suffers significant deviation from its path with increasing deflection angle for decreasing distance from the BH. In this section, we shall determine the deflection angle and lensing observables in the strong field regime for a static, spherically symmetric BH as described by the line element (6) [74,148,149], where the metric function $A(r)$ and $B(r)$ are connected as given by Eq. (7) and $C(r) = r^2$. Also, we will evaluate here the lensing observables for a few known supermassive BHs. It should be noted that as in the weak field limit, for this analysis also we confine the photon's entire trajectory in the equatorial plane ($\theta = \pi/2$) only.

4.1 Deflection angle

Both the deflection angle and lens equation are key factors for understanding the behavior of strong field gravitational lensing. In this scenario, a photon originating from a distant source and possessing a specific impact parameter is deflected by the BH as it reaches the closest approach distance r_0, which represents the turning point of its trajectory. Then it proceeds to the far-away observer in another direction [74,150–152]. As r_0 decreases, the deflection angle increases significantly. Once it reaches 2π, the photon makes a loop entirely around the BH before arriving at the observer [74,150]. Further decrease of r_0, the deflection angle exceeds 2π and the photon makes multiple loops around the BH before being escaped to infinity [74,153]. When r_0 approaches the photon sphere radius r_p the deflection angle diverges. For $r_0 < r_p$, the incoming photon gets trapped by the BH and cannot come out from it. However, one can rewrite the trajectory of the photon given by Eq. (14) in terms of radial effective potential $V_{eff}(r)$ as

$$\frac{V_{eff}(r)}{E^2} = \frac{\zeta^2}{r^2}\left[1 - \frac{2M}{r} + \frac{m^2}{12}\left(\frac{n-2}{2c_2}\right)^{1/n} r^2\right]. \tag{26}$$

Equation (26) determines different types of photon orbits namely, orbits with $\zeta < \zeta_p$, $\zeta = \zeta_p$ and $\zeta > \zeta_p$, where ζ_p is the impact parameter which is the critical or minimum impact parameter evaluated at the photon sphere radius r_p. A photon with an impact parameter smaller than ζ_p falls into the event horizon, whereas one with an impact parameter beyond the critical value ζ_p is scattered by the BH towards a distant observer. On the other hand, $\zeta = \zeta_p$ corresponds to a photon that follows a circular path of constant radius r_p, which becomes unstable by a small change in its radial position [153]. The potential of a photon sphere orbit is flat and satisfies the condition $V'_{eff}(r) = 0$. This condition leads

to the photon sphere equation [74,91,153] as

$$r A'(r) - 2A(r) = 0. \tag{27}$$

In fact, the photon sphere radius is the greatest positive root of Eq. (27) and in our case, it is found as $3M$ for the BH solution (7). Further, at $r = r_0$, the equation of orbit (14) yields the relation between the closest approach distance and the impact parameter as $\zeta_0 = \sqrt{C(r_0)/A(r_0)}$. From this, the critical impact parameter at $r_0 = r_p$ can be defined as [74,153]

$$\zeta_p = \sqrt{\frac{C(r_p)}{A(r_p)}}, \tag{28}$$

which for the BH solution (7) takes the form:

$$\zeta_p = \frac{r_p}{\sqrt{1 - \frac{2M}{r_p} + \frac{m^2}{12}\left(\frac{n-2}{2c_2}\right)^{1/n} r_p^2}}. \tag{29}$$

In strong deflection limit, the deviation suffered by a light ray is characterized by the deflection angle [74,148,154,155]

$$\hat{\alpha}(r_0) = I(r_0) - \pi, \tag{30}$$

where

$$I(r_0) = 2\int_{r_0}^{\infty} \frac{d\varphi}{dr}\, dr, \quad \frac{d\varphi}{dr} = \frac{\sqrt{B(r)}}{\sqrt{C(r)}\sqrt{\frac{C(r)A(r_0)}{C(r_0)A(r)} - 1}}. \tag{31}$$

To explore the behavior of the deflection angle we use the method developed by V. Bozza, applicable to light rays governed by a standard geodesic equation in any spacetime and under any gravitational theory [74]. He has evaluated the diverging deflection angle at $r_0 = r_p$ corresponding to an impact parameter $\zeta = \zeta_p$, by introducing a new variable z given as

$$z = \frac{A(r) - A(r_0)}{1 - A(r_0)}. \tag{32}$$

Using this variable, integral $I(r_0)$ can be expressed as [74, 86,153,156]

$$I(r_0) = \int_0^1 H(z, r_0)\, g(z, r_0)\, dz, \tag{33}$$

where the functions $H(z, r_0)$ and $g(z, r_0)$ are defined as [74]

$$H(z, r_0) = \frac{2\sqrt{C(r_0)}\,(1 - A(r_0))}{C(r)\,A'(r_0)}, \tag{34}$$

and

$$g(z, r_0) = \frac{1}{\sqrt{A(r_0) - \frac{A(r)}{C(r)}\,C(r_0)}}. \tag{35}$$

The function $H(z, r_0)$ is finite for all values of z and r_0, whereas $g(z, r_0)$ exhibits divergence as r_0 approaches the radius of the photon sphere, r_p. To estimate the rate of this divergence, the function within the square root in $g(z, r_0)$ is expanded to second-order in z that leads [74,153] the following relation:

$$g(z, r_0) \sim g_0(z, r_0) = \frac{1}{\sqrt{\psi(r_0)\, z + \eta(r_0)\, z^2}}, \tag{36}$$

with

$$\psi(r_0) = \frac{2\left(1 - \frac{3M}{r_0}\right)\left(\frac{2M}{r_0} - \frac{m^2}{12}\left(\frac{n-2}{2c_2}\right)^{1/n} r_0^2\right)}{\frac{2M}{r_0} + \frac{m^2}{6}\left(\frac{n-2}{2c_2}\right)^{1/n} r_0^2}, \tag{37}$$

$$\begin{aligned}\eta(r_0) = {} & \frac{\left(\frac{2M}{r_0} - \frac{m^2}{12}\left(\frac{n-2}{2c_2}\right)^{1/n} r_0^2\right)^2}{2\, r_0^4 \left(\frac{2M}{r_0^2} + \frac{m^2}{6}\left(\frac{n-2}{2c_2}\right)^{1/n} r_0\right)^3} \\ & \times \left[4\, r_0^3 \left(\frac{2M}{r_0^2} + \frac{m^2}{6}\left(\frac{n-2}{2c_2}\right)^{1/n} r_0\right)^2 \right. \\ & - \left(1 - \frac{2M}{r_0} + \frac{m^2}{12}\left(\frac{n-2}{2c_2}\right)^{1/n} r_0^2\right) \\ & \left. \times \left(4M + \frac{4m^2}{3}\left(\frac{n-2}{2c_2}\right)^{1/n} r_0^3\right)\right].\end{aligned} \tag{38}$$

Also, the variable z in Hu–Sawicki model BH takes the form:

$$z = 2M\left(\frac{r - r_0}{r r_0}\right) + \frac{m^2}{12}\left(\frac{n-2}{2c_2}\right)^{1/n}\left(r^2 - r_0^2\right). \tag{39}$$

At $r_0 = r_p$, the coefficient $\psi(r_0)$ of z becomes zero that makes $g_0(z, r_0)$ to behave as z^{-1} resulting a logarithmic divergence of the integral (33). Moreover, the integral $I(r_0)$ can be solved by dividing it into the divergent and regular terms as [74]

$$I(r_0) = I_D(r_0) + I_R(r_0), \tag{40}$$

where

$$I_D(r_0) = \int_0^1 H(0, r_p)\, g_0(z, r_0)\, dz, \tag{41}$$

$$I_R(r_0) = \int_0^1 \left[H(z, r_0)\, g(z, r_0) - H(0, r_p)\, g_0(z, r_0)\right] dz.$$

(42)

Further analysis of integrals (41) and (42) in strong field limit and approximating them using the leading terms an analytical expression for the deflection angle in terms of impact parameter near the point of divergence can be established in the following form [74]:

$$\hat{\alpha}(\zeta) = -\bar{a}\log\left(\frac{\zeta}{\zeta_p} - 1\right) + \bar{b} + \mathcal{O}(\zeta - \zeta_p), \tag{43}$$

where the strong deflection coefficients $\bar{a}$ and $\bar{b}$ are given as

$$\bar{a} = \frac{a}{2} = \frac{H(0, r_p)}{2\sqrt{\eta(r_p)}}, \tag{44}$$

$$\bar{b} = -\pi + b_R + b_D, \tag{45}$$

where

$$b_D = \bar{a}\,\log\left[2\,\eta(r_p)\left(\frac{m^2}{12}\,r_p^2\left(\frac{n-2}{2c_2}\right)^{1/n} - \frac{2M}{r_p} + 1\right)^{-1}\right], \tag{46}$$

$$b_R = I_R(r_p) = \int_0^1 \big[H(z, r_p)\,g(z, r_p) - H(0, r_p)\,g_0(z, r_p)\big]\,dz, \tag{47}$$

and $\zeta_p = \zeta(r_p)$ as given by Eq. (29). We proceed by utilizing Eq. (43) to obtain the strong deflection angle for the BH under consideration. To do this, we first calculate $\bar{a}$ employing Eq. (44), followed by computing b_D based on $\eta(r_p)$ and $\bar{a}$ as specified in Eqs. (38) and (44) respectively at $r_0 = r_p$. The integral b_R represented by Eq. (47) is estimated numerically where Eqs. (35) and (36) are used along with Eq. (32). Employing all these values into Eq. (43) we obtain the deflection angle for our BH (7). To examine the behavior of the deflection angle, we depict its variation with impact parameter ζ for different values of model parameters with $M = 1$ in Fig. 5, where the left plot is for different values c_2 fixing $m = 0.5$ and the right one is for changing values of m by keeping $c_2 = 1.5$ for all. Another model parameter n is taken as 0.5 for both cases. The figure demonstrates the increase in the deflection angle as the impact parameter decreases, then diverging to reach the observer at $\zeta = \zeta_p$. Additionally, according to the left plot as c_2 increases, the point of divergence shifts to higher values of impact parameter i.e., the light diverges at greater ζ_p value for the larger c_2, thereby approaching the characteristics of Schwarzschild BH. In contrast, it is evident from the right plot that for smaller values of m, the deflection angle remains close to that of the Schwarzschild case and shows a gradual deviation from the angle as m increases. The deflection angle is seen to move towards the negative end typically as mentioned in the weak lensing case for larger m and the smaller c_2 values respectively. Notably, Fig. 5 demonstrates that the Hu–Sawicki BHs possess smaller ζ_p values than that of the Schwarzschild BH for any value on model parameters. This suggests the induction of a weaker gravitational field of the Hu–Sawicki BHs due to modification as compared to the Schwarzschild BH.

The coefficients $\bar{a}$ and $\bar{b}$ rely on metric functions calculated at r_p which in Schwarzschild's case are found to be equal to 1 and -0.400841 respectively. To illustrate the behavior of coefficients $\bar{a}$ and $\bar{b}$, we present their graphical representation as functions of the model parameters c_2 and m collectively in Fig. 6. The figure illustrates that initially $\bar{a}$ increases with increasing the model parameters, reaches a peak, then falls and finally remains constant beyond certain parameter values. In contrast, the initial behavior of $\bar{b}$ is different with respect to parameters c_2 and m. $\bar{b}$ increases initially with respect to c_2, but decreases initially for the parameter m. However, as in the case of the parameter m, $\bar{b}$ decreases after a particular value of c_2 and then for both cases it increases after attaining a sufficiently smaller value. It becomes constant as the model parameters grow. This type of behavior of $\bar{a}$ and $\bar{b}$ is also found in the Simpson–Visser black-bounce spacetime as described in Ref. [157] (Fig. 7).

4.2 Lensing observables

From the deflection angle calculated in the strong field limit, the properties of relativistic images can be obtained using a lens equation that relates the position of the source and images formed by the lensing object. The formation of the relativistic images is due to the spiraled light rays around the BH in the strong gravitational field and are significantly demagnified relative to the standard weak field images unless there is a strong alignment of the source, lens, and observer [76,87,92]. In the case of a highly aligned configuration (see Fig. 9), the lens equation can be expressed as follows [74,76,86,87,152,155]:

$$\beta = \vartheta - \frac{d_{ls}}{d_{os}}\,\Delta\alpha_k, \tag{48}$$

where β and ϑ represent the angular separation between the lens and the source, and the lens and the image respectively. $\Delta\alpha_k = \hat{\alpha} - 2k\pi$, with k as a positive integer represents a winding number of light rays in multiple loops around the BH. d_{ls} and d_{os} are distances of the lens (BH) from the source and the observer respectively. Using Eqs. (43), (48) and the relation $\zeta \approx \vartheta\, d_{ol}$, the angular position ϑ_k of k^{th} relativistic image can be expressed as [59,151,152,155]

$$\vartheta_k = \vartheta_k^0 + \Delta\vartheta_k, \tag{49}$$

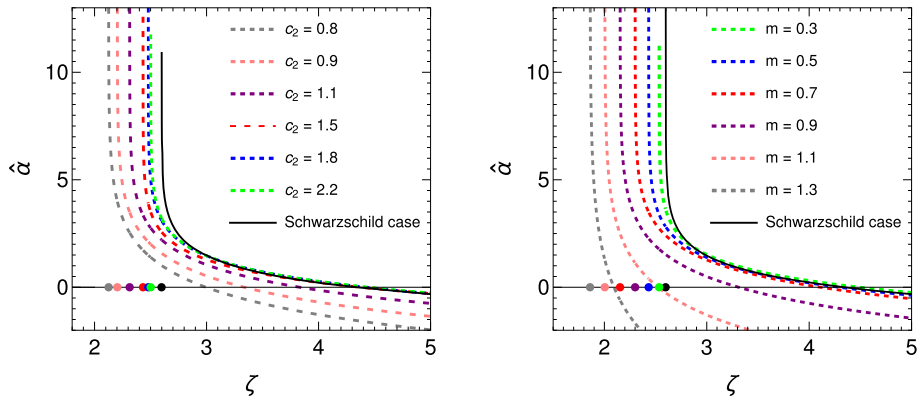

Fig. 5 Variation of deflection angle with impact parameter ζ for different values of the Hu–Sawicki model parameters where the points on the horizontal axis represent the value of impact parameter $\zeta = \zeta_p$ at which the deflection angle diverges. The model parameters $m = 0.5$ and $c_2 = 1.5$ are considered for the left and right panels respectively with $M = 1$ and $n = 0.5$ in both cases

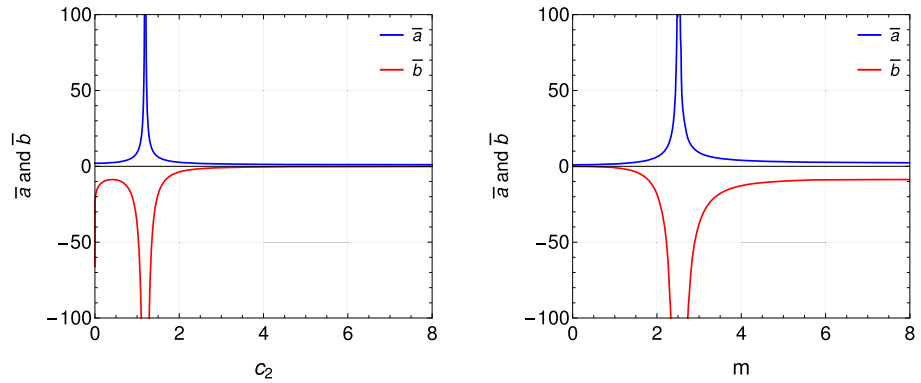

Fig. 6 Variation of $\bar{a}$ and $\bar{b}$ with model parameters c_2 and m for $M = 1, n = 0.5$. The blue and red curves represent $\bar{a}$ and $\bar{b}$ respectively

where ϑ_k^0 represents the image position corresponding to $\hat{\alpha} = 2k\pi$ when a photon winds complete $2k\pi$ around the BH, and is found as [74,86,152]

$$\vartheta_k^0 = \frac{\zeta_p}{d_{ol}}(1 + e_k), \tag{50}$$

and

$$\Delta\vartheta_k = \frac{(d_{ol} + d_{ls})\,\zeta_p\, e_k}{\bar{a}\, d_{ls} d_{ol}}\,(\beta - \vartheta_k^0), \tag{51}$$

$$e_k = \exp\left(\frac{\bar{b} - 2k\pi}{\bar{a}}\right). \tag{52}$$

Thus Eq. (49) can be approximated as [74,76,77,152]

$$\vartheta_k = \vartheta_k^0 + \frac{\zeta_p e_k(\beta - \vartheta_k^0) d_{os}}{\bar{a}\, d_{ls} d_{ol}}. \tag{53}$$

This equation links the position of relativistic images with the lensing coefficients $\bar{a}$, $\bar{b}$ and critical impact parameter ζ_p. From Eq. (50) we can evaluate ϑ_∞, the asymptotic position of a set of images. Since as $k \to \infty$, e_k approaches zero, thereby the equation results in $\vartheta_\infty = \frac{\zeta_p}{d_{ol}}$ [76,152]. Furthermore, treating ϑ_1 as a single-loop outermost relativistic image and ϑ_∞ as a pack of all inner ones, the angular separation s between these two can be obtained as [74,76,79,153]

$$s = \vartheta_1 - \vartheta_\infty = \vartheta_\infty \exp\left(\frac{\bar{b} - 2\pi}{\bar{a}}\right). \tag{54}$$

Another important characteristic observable in strong gravitational lensing is the magnification of relativistic images which is the inverse of the Jacobian determinant evaluated at the position of the image and is given for k^{th} image as [74,76,154,158]

$$\mu_k = \left(\frac{\beta}{\vartheta}\frac{\partial\beta}{\partial\vartheta}\right)^{-1}\Bigg|_{\vartheta_k^0} \simeq \frac{e_k(1 + e_k) d_{os}}{\bar{a}\,\beta\, d_{ls}\, d_{ol}^2}\,\zeta_p^2. \tag{55}$$

It is evident from the above equation that μ_k is an inverse function of d_{ol}^2. Therefore, it is quite small which makes the relativistic images usually dim except for $\beta \to 0$ because this limiting condition leads to an almost perfect alignment

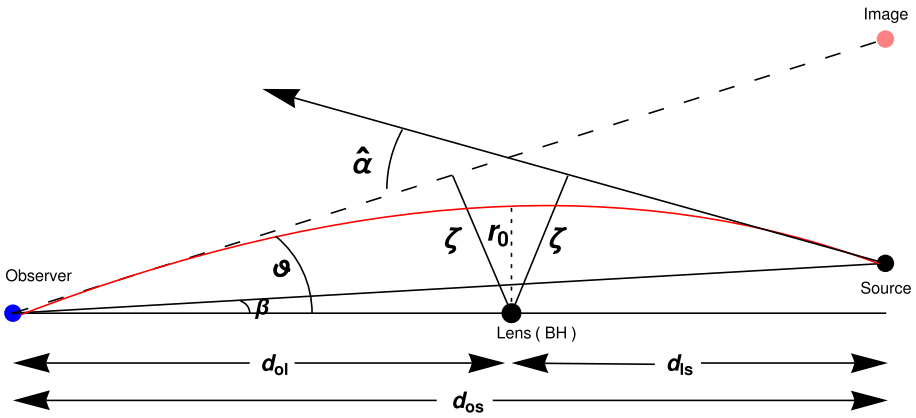

Fig. 7 A schematic diagram of strong gravitational lensing

of the source, observer and lens. In conjunction with Eq. (55) the ratio of magnification $r_{\rm mag}$ of the outermost relativistic image at ϑ_1 to remaining packed inner images at ϑ_∞ can be found as [86,152]

$$r_{\rm mag} = \frac{\mu_1}{\sum_{k=2}^{\infty}\mu_k} = \exp\left(\frac{2\pi}{\bar{a}}\right). \tag{56}$$

Interestingly, this observable is independent of mass and the distance between the BH and the observer. In the following subsection, we will consider observational data of two supermassive BHs Sgr A* and M87* to compute the values of lensing coefficients numerically predicted by the Hu–Sawicki BH.

4.3 Evaluation of observables from supermassive BHs

We assume that the gravitational fields of the supermassive BHs Sgr A* at the centers of our galaxy and M87* in Messier 87 galaxy are characterized by the Hu–Sawicki BHs within the framework of $f(R)$ gravity theory. We compute the numerical values of key observables such as angular position ϑ_∞, angular separation s, and relative magnification $r_{\rm mag}$ related to gravitational lensing in the strong field limit to investigate the impact of model parameters on the lensing effect. For this, we employ the mass $M = 4.3 \times 10^6 M_\odot$ of Sgr A* and its distance $d_{ol} = 8.35$ kpc from the Earth based on Refs. [61,86,159–161]. Similarly, in the case of $M87^*$, a mass $M = 6.5 \times 10^9 M_\odot$ and a distance $d_{ol} = 16.8$ Mpc are adopted following the data in the Refs. [4,61,86]. The numerically calculated the characteristic lensing observables ϑ_∞, s and $r_{\rm mag}$ across different values of model parameters m and c_2 for both the BHs are presented in Figs. 8 and 9, and tabulate in Table 1. Figure 8 shows that ϑ_∞ decreases with increasing m and almost remains unaltered for larger m. Contrary to this, it increases steeply with increasing c_2 initially and becomes constant once c_2 attains a certain value. Meanwhile, the relative magnitude $r_{\rm mag}$ displays almost a similar pattern in both cases of varying m and c_2. It decreases first for a small range of the values of parameters and then rises to a fixed value across the greater range of parameters in both cases. It is seen that the fall and rise of $r_{\rm mag}$ with parameter m is shallower than that for the variation with c_2. In addition, Table 1 highlights the differences in the values of ϑ_∞, s and $r_{\rm mag}$ produced by the Hu–Sawicki model in comparison to the Schwarzschild case. The table shows that the minimum angular position ϑ_∞ reaches 16.4892 μas for Sgr A* and 12.3665 μas for $M87^*$ in the Hu–Sawicki case whereas ϑ_∞ in Schwarzschild case for these respective BHs are 26.5972 and 19.9473 respectively. Thus, one may find deviations $\Delta\vartheta_\infty$ as 9.7480 μas and 7.5808 μas for these two respective BHs. On the other hand, in Fig. 9 we jointly depict the behavior of observable s with parameters m and c_2 respectively for the BHs SgrA* and M87*. Observation reveals that s shows a bimodal behavior initially following an attenuated pattern and then decreases as m increases. Contrarily, in the case of c_2 variations, a bimodal pattern with increasing peak value is observed with a flattened behavior in the large parameter value. The figure also clearly indicates a small angular separation between SgrA* and M87* for both m and c_2.

5 Conclusion

Gravitational lensing is a significant tool for probing the nature of BHs across various gravity theories. In this work, we have analyzed the gravitational lensing phenomenon in both the weak and strong field lensing regimes in the light of BHs governed by the Hu–Sawicki model in the framework of the $f(R)$ gravity theory. The deflection angle and the lensing properties of such BHs have been investigated in the weak field limit by employing the extended form of the GBT developed by Ishihara et al. [114] and in the strong field limit by employing a widely recognized technique proposed by V. Bozza [74].

Table 1 Estimation of numerical values of characteristic strong lensing observables along with lensing coefficients and corresponding impact parameter ζ_p for the BHs SgrA* and M87*. Here r_s refers to the Schwarzschild radius

m	c_2	SgrA* $\vartheta_\infty(\mu$as)	SgrA* s (μas)	M87* $\vartheta_\infty(\mu$as)	M87* s (μas)	$r_{\rm mag}$	ζ_p/r_s	$\bar{a}$	$\bar{b}$
0	0	26.5972	0.033239	19.9473	0.024820	6.77155	2.59808	1.00000	−0.40084
0.5	0.8	21.7573	0.027190	16.3175	0.020392	4.08529	2.12530	1.65754	−1.48220
	1.1	23.6806	0.029594	17.7600	0.022194	5.13907	2.31311	1.31766	−0.55410
	1.5	24.9037	0.031123	18.6772	0.023341	5.81554	2.43265	1.04527	−0.23514
	2.2	25.7683	0.032203	19.3256	0.024151	6.30025	2.50104	1.07481	−0.27168
0.7	0.8	18.9546	0.023687	14.2155	0.017765	2.52765	1.85153	2.70229	−5.75272
	1.1	21.6264	0.027027	16.2193	0.020269	4.04836	2.11252	1.68721	−1.24456
	1.5	23.5491	0.029429	17.6613	0.022071	5.11085	2.30033	1.33646	−0.59376
	2.2	25.0413	0.031294	18.7804	0.023470	5.89223	2.44609	1.14923	−0.29789
0.9	0.8	16.4892	0.020607	12.3665	0.015454	0.91525	1.61070	7.46295	−33.8099
	1.1	19.5693	0.024456	14.6765	0.018341	2.88859	1.91157	2.36462	−4.22514
	1.5	22.0451	0.027550	16.5333	0.020662	4.27993	2.15341	1.59592	−1.28673
	2.2	24.1612	0.030195	18.1204	0.022645	5.45080	2.36012	1.25311	−0.43259

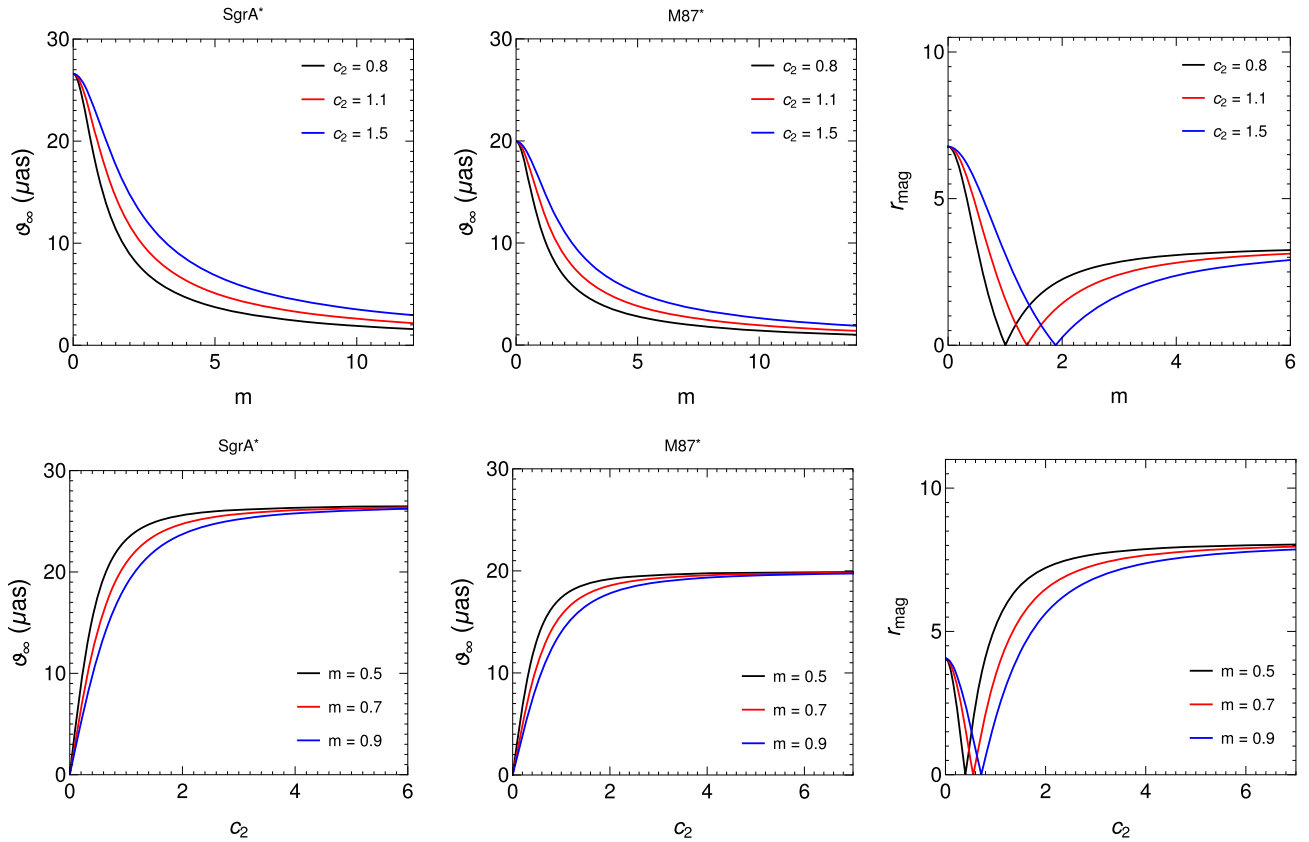

Fig. 8 Variation of strong lensing observables ϑ_∞ and $r_{\rm mag}$ with respect to parameters m and c_2 for BHs Sgr A* and M87*. The left two plots present the change of ϑ_∞ for Sgr A*, middle two plots depict the corresponding change for M87* while the right plots show the variation of relative magnitude $r_{\rm mag}$. It is to be noted that $r_{\rm mag}$ is not any BH specific

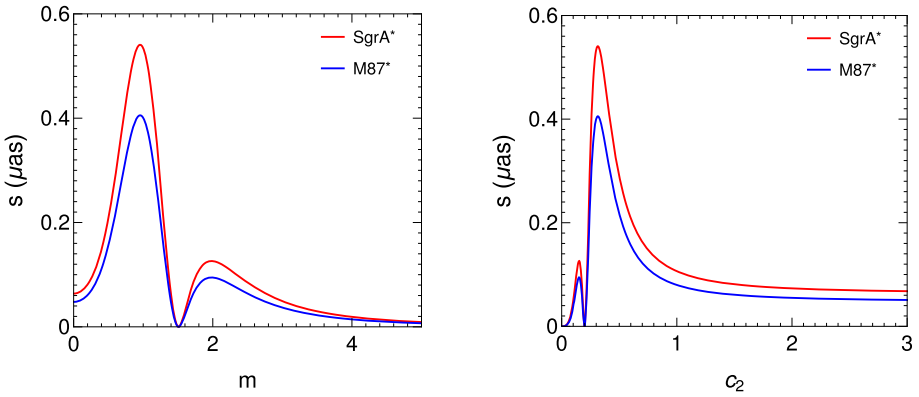

Fig. 9 Behavior of s with parameters m and c_2 for BHs Sgr A* and M87*. The left panel illustrates the variation of s with m keeping c_2 fixed at 1.5, and the right panel shows the variation of s with c_2 keeping $m = 0.5$

In the first part of our work, we investigate the bending angle of light in the weak field limit. The approach employed in this scenario is the extension of the GBT developed by Ishihara et al. to deduce the deflection angle of light in the weak field of the BH under study from the viewpoint of the receiver. This approach is independent of the asymptotic flatness of the spacetime in which it is employed. As a result, we applied this method to the asymptotically non-flat BH in the Hu–Sawicki model $f(R)$ gravity. Thus, to examine the bending of light in this type of BHs we focus on how the deflection angle varies with the impact parameter along with the variation of model parameters c_2 and m through graphical analyses. It is seen from the analyses that there is a distinct deviation from the Schwarzschild case, particularly at larger impact parameters where the deflection angle becomes negative. Higher values of c_2 lead the deflection angle closer to the Schwarzschild behavior, though it remains negative at large impact parameters. Oppositely, lower values of m allow the recovery of the Schwarzschild behavior and show near alignment with $m = 0.05$ even at large impact parameter values. Our study has revealed that the model parameters have a significant effect on the deflection angle and give us an idea about the gravitational nature of the BHs.

In the next part, we have analyzed how the deflection of a light ray around the Hu–Sawicki BHs depends on the impact parameter ζ by plotting $(\hat{\alpha} - \zeta)$ graph in the strong field limit by varying parameters c_2 and m at $M = 1, n = 0.5$, and found that corresponding to a particular impact parameter the deflection angle increases with the decrease of the impact parameter value and shows divergence at the photon sphere as expected. Additionally, it is observed that deflection angles of Hu–Sawiki BHs move away from the Schwarzschild case as parameter m increases but approach it with increasing the parameter c_2 taking on negative values at larger impact parameters similar to the weak lensing case. Of course, the negative values in the strong lensing limit naturally appear at smaller impact parameters compared to the weak lensing scenario. The occurrence of the negative deflection angle at large impact parameters suggests photon repulsion by the black hole's gravitational field, indicating a significant influence of the Hu–Sawicki $f(R)$ gravity on the gravitational lensing phenomenon. We have analyzed the behavior of strong lensing coefficients $\bar{a}$ and $\bar{b}$ in Hu–Sawicki spacetime and seen that $\bar{a}$ and $\bar{b}$ exhibit intricate behavior with stabilization at larger values of model parameters.

We then extend our analysis to the supermassive BHs Sgr A* and M87* as the models of Hu–Sawicki BHs to numerical estimation of the basic observables ϑ_∞, s and $r_{\rm mag}$ related to the strong gravitational lensing effect. For this purpose, the mass and distance parameters of these objects as reported by EHT group [3,160] are used. The results thus obtained are listed in Table 1 as mentioned which tells us that the modification of BHs spacetime by Hu–Sawicki $f(R)$ gravity reduces the value of ϑ_∞ relative to GR (Schwarzschild case). The amount of reduction depends sensitively on the parameters of the model. Thus, our findings reveal that the lensing observables exhibit notable sensitivity to the variation in model parameters. Specifically, ϑ_∞ decreases as m increases, while it experiences a steep rise with c_2 before stabilization. Contrarily, s and $r_{\rm mag}$ display intricate variation with gradual flattening across higher parameter values. Finally, we may note that our work provides significant evidence that the Hu–Sawicki model introduces notable gravitational lensing signatures and demonstrates considerable deviations from the Schwarzschild case. Indeed, our analysis highlights how gravitational lensing in both weak and strong regimes can be utilized to investigate BH metrics within modified gravity theories. These studies can be extended to wormhole backgrounds in different gravity theories as a future prospect.

Acknowledgements UDG is thankful to the Inter-University Centre for Astronomy and Astrophysics (IUCAA), Pune, India for the Visiting Associateship of the institute.

Data Availability Statement This manuscript has no associated data. [Author's' comment: Data sharing not applicable to this article as no datasets were generated or analysed during the current study.]

Code Availability Statement This manuscript has no associated code/software. [Author's comment: Code/Software sharing not applicable to this article as no code/software was generated or analysed during the current study.]

Funded by SCOAP[3].

References

1. A. Einstein, The foundation of the general theory of relativity. Ann. Phys. (N. Y.) **49**, 769 (1916). https://doi.org/10.1002/andp.19163540702
2. A. Einstein, The foundation of the general theory of relativity. Ann. Phys. (N. Y.) **14**, 517 (2005). https://doi.org/10.1002/andp.19163540702
3. K. Akiyama et al. (Event Horizon Telescope), First M87 Event Horizon Telescope results. I. The shadow of the supermassive black hole, Astrophys. J. Lett. **875**, L1 (2019). https://doi.org/10.3847/2041-8213/ab1141
4. K. Akiyama et al. (Event Horizon Telescope), First Sagittarius A* Event Horizon Telescope results. I. The shadow of the supermassive black hole in the Center of the Milky Way, Astrophys. J. Lett. **930**, L12 (2022). https://doi.org/10.3847/2041-8213/ac6674
5. B.P. Abbott et al., Observation of gravitational waves from a binary black hole merger. Phys. Rev. Lett. **116**, 061102 (2016). https://doi.org/10.1103/PhysRevLett.116.061102
6. B.P. Abbott et al., GW170817: observation of gravitational waves from a binary neutron star Inspiral. Phys. Rev. Lett. **119**, 161101 (2017). https://doi.org/10.1103/PhysRevLett.119.161101
7. A.G. Reiss et al., Observational Evidence from Supernovae for an Accelerating Universe and a Cosmological Constant. Astron. J. **116**, 1009 (1998). https://doi.org/10.1086/300499
8. S. Perlmutter et al., Measurements of Ω and Λ from 42 High-Redshift Supernovae. Astrophys. J. **517**, 565 (1999). https://doi.org/10.1086/307221
9. V.C. Rubin, N. Thonnard, W.K. Ford Jr., Rotational properties of 21 SC galaxies with a large range of luminosities and radii, from NGC 4605 (R = 4 kpc) to UGC 2885 (R = 122 kpc). Astrophys. J. **238**, 471–487 (1980)
10. Bing-Lin. Young, A survey of dark matter and related topics in cosmology. Front. Phys. **12**, 121201 (2017). https://doi.org/10.1007/s11467-016-0583-4
11. N. Parbin, U.D. Goswami, Galactic rotation dynamics in a new $f(\mathcal{R})$ gravity model. EPJC **83**, 411 (2023). https://doi.org/10.1140/epjc/s10052-023-11568-x
12. G. Mohan, U.D. Goswami, Galactic rotation curves of spiral galaxies and dark matter in $f(R,T)$ gravity theory. IJGMMP **21**, 2450082 (2024). https://doi.org/10.1142/S0219887824500828
13. G. Mohan, U.D. Goswami, Galactic dynamics in the presence of scalaron: a perspective from f (R) gravity. Phys. Scr. **99**, 095025 (2024). https://doi.org/10.1088/1402-4896/ad6d0d
14. G. Bertone, D. Hooper, History of dark matter. Rev. Mod. Phys. **90**, 045002 (2018). https://doi.org/10.1103/RevModPhys.90.045002
15. J.G. de Swart, G. Bertone, J. van Dongen, How dark matter came to matter. Nat. Astron. **1**, 0059 (2017). https://doi.org/10.1038/s41550-017-0059
16. K. Garrett, G. Duda, Dark matter: a primer. Adv. Astron. **2011**, 968283 (2011). https://doi.org/10.1155/2011/968283
17. S.W. Hawking, The occurrence of singularities in cosmology III. Proc. R. Soc. Lond. **A300**, 187–201 (1967). https://doi.org/10.1098/rspa.1967.0164
18. S.W. Hawking, G.F.R. Ellis, The Large Scale Structure of Space-time (CUP, 1973). https://doi.org/10.1017/9781009253161
19. T. Clifton et al., Modified gravity and cosmology. Phys. Rep. **513**, 1–189 (2012). https://doi.org/10.1016/j.physrep.2012.01.001
20. T. Clifton, Alternative Theories of Gravity (2006). arXiv:gr-qc/0610071
21. S. Capozziello, M. De Laurentis, Extended theories of gravity. Phys. Rep. **509**, 167 (2011). https://doi.org/10.1016/j.physrep.2011.09.003
22. S. Nojiri, S.D. Odintsov, Unified cosmic history in modified gravity: from F(R) theory to Lorentz non-invariant models. Phys. Rep. **505**, 59 (2011). https://doi.org/10.1016/j.physrep.2011.04.001
23. S. Nojiri, S.D. Odintsov, Dark energy, inflation and dark matter from modified F(R) gravity. TSPU Bull. **N8**(110), 7–19 (2011)
24. S. Nojiri, S.D. Odintsov, V.K. Oikonomou, Modified gravity theories on a nutshell: inflation, bounce and late-time evolution. Phys. Rep. **692**, 1 (2017). https://doi.org/10.1016/j.physrep.2017.06.001
25. V. Faraoni, Cosmology in scalar-tensor gravity. Fundam. Theor. Phys. (2004). https://doi.org/10.1007/978-1-4020-1989-0
26. J.W. Moffat, Scalar-tensor-vector gravity theory. JCAP **2006**, 004 (2006). https://doi.org/10.1088/1475-7516/2006/03/004
27. S. Bahamonde, C.G. Böhmer, M. Wright, Modified teleparallel theories of gravity. Phys. Rev. D **92**, 104042 (2015). https://doi.org/10.1103/PhysRevD.92.104042
28. S. Bahamonde et al., Teleparallel gravity: from theory to cosmology. Rep. Prog. Phys. **86**, 026901 (2023). https://doi.org/10.1088/1361-6633/ac9cef
29. F. Canfora et al., General relativity from Einstein—Gauss-Bonnet gravity. Phys. Rev. D **104**, 044026 (2021). https://doi.org/10.1103/PhysRevD.104.044026
30. T.P. Sotiriou, V. Faraoni, f(R) theories of gravity. Rev. Mod. Phys. **82**, 451 (2010). https://doi.org/10.1103/RevModPhys.82.451
31. A. De Felice, S. Tsujikawa, F(R) theories. Living Rev. Relativ. **13**, 3 (2010). https://doi.org/10.12942/lrr-2010-3
32. G.J. Olmo, Palatini approach to modified gravity: F(R) theories and beyond. Int. J. Mod. Phys. D **20**, 413 (2011). https://doi.org/10.1142/S0218271811018925
33. V. Vikram et al., Astrophysical tests of modified gravity: stellar and gaseous rotation curves in Dwarf Galaxies. Phys. Rev. D **97**, 104055 (2018). https://doi.org/10.1103/PhysRevD.97.104055
34. V.K. Sharma, B.K. Yadav, M.M. Verma, Extended galactic rotational velocity profiles in f(R) gravity background. EPJC **80**, 619 (2020). https://doi.org/10.1140/epjc/s10052-020-8186-1
35. N. Parbin, U.D. Goswami, Scalarons mimicking dark matter in the Hu–Sawicki model of f(R) gravity. Mod. Phys. Lett. A **36**, 2150265 (2021). https://doi.org/10.1142/S0217732321502655
36. A.P. Naik et al., Imprints of chameleon f(R) gravity on galaxy rotation curves. Mon. Not. R. Astron. Soc. **480**, 5211 (2018). https://doi.org/10.1093/mnras/sty2199
37. B. Li, M. Shirasaki, Galaxy–Galaxy weak gravitational lensing in f(R) gravity. Mon. Not. R. Astron. Soc. **474**, 3599 (2018). https://doi.org/10.1093/mnras/stx3006
38. A. Errehymy et al., Possible wormholes in $f(R)$ gravity sourced by solitonic quantum wave and cold dark matter halos and their repulsive gravity effect. (2024). arXiv:2408.07667
39. A. Guilabert et al., Static and spherically symmetric vacuum spacetimes with non-expanding principal null directions in f(R) gravity. Eur. Phys. J. C **84**, 678 (2024). https://doi.org/10.1140/epjc/s10052-024-13063-3

40. A. Talukdar, S. Kalita, Big Bang nucleosynthesis with f(R) gravity scalarons and astrophysical consequences. ApJ **970**, 91 (2024). https://doi.org/10.3847/1538-4357/ad5843
41. A.A. Starobinsky, Disappearing cosmological constant in f(R) gravity. JETP Lett. **86**, 157 (2007). https://doi.org/10.1134/S0021364007150027
42. W. Hu, I. Sawicki, Models of f(R) cosmic acceleration that evade solar system tests. Phys. Rev. D **76**, 064004 (2007). https://doi.org/10.1103/PhysRevD.76.064004
43. J.Y. Cen et al., Cosmological evolutions in Tsujikawa model of f(R) gravity. Phys. Dark Univ. **26**, 100375 (2019)
44. D.J. Gogoi, U.D. Goswami, A new f(R) gravity model and properties of gravitational waves in it. EPJC **80**, 1101 (2020). https://doi.org/10.1140/epjc/s10052-020-08684-3
45. T. Katsuragawa, S. Matsuzaki, Cosmic history of chameleonic dark matter in F(R) gravity. Phys. Rev. D **97**, 064037 (2018). https://doi.org/10.1103/PhysRevD.97.064037
46. T. Katsuragawa, S. Matsuzaki, E. Senaha, F(R) gravity in the early Universe: electroweak phase transition and chameleon mechanism*. Chin. Phys. C **43**, 105101 (2019). https://doi.org/10.1088/1674-1137/43/10/105101
47. P. Bessa, M. Campista, A. Bernui, Observational constraints on Starobinsky f(R) cosmology from cosmic expansion and structure growth data. EPJC **82**, 506 (2022). https://doi.org/10.1140/epjc/s10052-022-10457-z
48. J. Bora, D.J. Gogoi, U.D. Goswami, Strange stars in f(R) gravity Palatini formalism and gravitational wave echoes from them. JCAP **09**, 057 (2022). https://doi.org/10.1088/1475-7516/2022/09/057
49. F.W. Dyson et al., IX. A determination of the deflection of light by the sun's gravitational field, from observations made at the total eclipse of May 29, 1919. Philos. Trans. R. Soc. A **220**, 291 (1920). https://doi.org/10.1098/rsta.1920.0009
50. P.S. Schneider, J. Ehlers, E. Falco, *Gravitational Lenses* (Springer, Berlin, 1992). https://doi.org/10.1007/978-3-662-03758-4
51. P. Schneider, C.S. Kochanek, J. Wambsganss, *Gravitational Lensing: Strong, Weak, and Micro* (Springer, Berlin, 2006)
52. M. Bartelmann, Gravitational lensing. Class. Quantum Gravity **27**, 233001 (2010). https://doi.org/10.1088/0264-9381/27/23/233001
53. J. Wambsganss, Gravitational lensing in astronomy. Living Rev. Relativ. **1**, 12 (1998). https://doi.org/10.12942/lrr-1998-12
54. R.D. Blandford, R. Narayan, Cosmological applications of gravitational lensing. Annu. Rev. Astron. Astrophys. **30**, 311 (1992). https://doi.org/10.1146/annurev.aa.30.090192.001523
55. A.B. Congdon, C.R. Keeton, *Principles of Gravitational Lensing: Light Deflection as a Probe of Astrophysics and Cosmology* (Springer International Publishing, Cham, 2018). https://doi.org/10.1007/978-3-030-02122-1
56. E.F. Eiroa, G.E. Romero, D.F. Torres, Reissner–Nordström black hole lensing. Phys. Rev. D **66**, 024010 (2002). https://doi.org/10.1103/PhysRevD.66.024010
57. G.N. Gyulchev, S.S. Yazadjiev, Kerr–Sen dilaton-axion black hole lensing in the strong deflection limit. Phys. Rev. D **75**, 023006 (2007). https://doi.org/10.1103/PhysRevD.75.023006
58. S.S. Zhao, Y. Xie, Strong field gravitational lensing by a charged galileon black hole. JCAP **2016**, 007 (2016) https://iopscience.iop.org/article/10.1088/1475-7516/2016/07/007
59. S.S. Zhao, Y. Xie, Strong deflection gravitational lensing by a modified Hayward black hole. EPJC **77**, 272 (2017). https://doi.org/10.1140/epjc/s10052-017-4850-5
60. R. Kumar, S.U. Islam, S.G. Ghosh, Gravitational lensing by charged black hole in regularized 4D Einstein–Gauss–Bonnet gravity. EPJC **80**, 1128 (2020). https://doi.org/10.1140/epjc/s10052-020-08606-3
61. Y. Dong, The gravitational lensing by rotating black holes in loop quantum gravity. Nucl. Phys. B **1005**, 116612 (2024). https://doi.org/10.1016/j.nuclphysb.2024.116612
62. N. Parbin, D.J. Gogoi, U.D. Goswami, Weak gravitational lensing and shadow cast by rotating black holes in axionic Chern–Simons theory. Phys. Dark Univ. **41**, 101265 (2023). https://doi.org/10.1016/j.dark.2023.101265
63. N. Parbin et al., Deflection angle, quasinormal modes and optical properties of a de sitter black hole in f(T, B) gravity. Phys. Dark Univ. **42**, 101315 (2023). https://doi.org/10.1016/j.dark.2023.101315
64. H. Lekbich et al., The optical features of noncommutative charged 4D-AdS-Einstein–Gauss–Bonnet black hole: shadow and deflection angle. EPJC **84**, 350 (2024). https://doi.org/10.1140/epjc/s10052-024-12728-3
65. S. Sahu, K. Lochan, D. Narasimha, Gravitational lensing by self-dual black holes in loop quantum gravity. Phys. Rev. D **91**, 063001 (2015). https://doi.org/10.1103/PhysRevD.91.063001
66. A.R. Soares, R.L.L. Vitória, C.F.S. Pereira, Gravitational lensing in a topologically charged Eddington-inspired Born–Infeld spacetime. EPJC **83**, 903 (2023). https://doi.org/10.1140/epjc/s10052-023-12071-z
67. J. Badía, E.F. Eiroa, Gravitational lensing by a Horndeski black hole. EPJC **77**, 779 (2017). https://doi.org/10.1140/epjc/s10052-017-5376-6
68. S. Vagnozzi et al., Horizon-scale tests of gravity theories and fundamental physics from the Event Horizon Telescope image of Sagittarius A*. Class. Quantum Gravity **40**, 165007 (2023). https://doi.org/10.1088/1361-6382/acd97b
69. R.C. Pantig, A. Övgün, Testing dynamical torsion effects on the charged black hole's shadow, deflection angle and greybody with M87* and SgrA* from EHT. Ann. Phys. **448**, 169197 (2023). https://doi.org/10.1016/j.aop.2022.169197
70. D. Clowe et al., A direct empirical proof of the existence of dark matter. ApJ **648**, L109 (2006). https://doi.org/10.1086/508162
71. R. Massey, T. Kitching, J. Richard, The dark matter of gravitational lensing. Rep. Prog. Phys. **73**, 086901 (2010). https://doi.org/10.1088/0034-4885/73/8/086901
72. Z. Fu, S. Gao, The application of gravitational lensing on observation of dark matter candidates. J. Phys. Conf. Ser. **2386**, 012076 (2022). https://doi.org/10.1088/1742-6596/2386/1/012076
73. C.G. Darwin, The gravity field of a particle. Proc. R. Soc. Lond. A **249**, 180 (1959). https://doi.org/10.1098/rspa.1959.0015
74. V. Bozza, Gravitational lensing in the strong field limit. Phys. Rev. D **66**, 103001 (2002). https://doi.org/10.1103/PhysRevD.66.103001
75. V. Bozza, Quasiequatorial gravitational lensing by spinning black holes in the strong field limit. Phys. Rev. D **67**, 103006 (2003). https://doi.org/10.1103/PhysRevD.67.103006
76. R. Whisker, Strong gravitational lensing by braneworld black holes. Phys. Rev. D **71**, 064004 (2005). https://doi.org/10.1103/PhysRevD.71.064004
77. S. Chen, J. Jing, Strong field gravitational lensing in the deformed Hořava–Lifshitz black hole. Phys. Rev. D **80**, 024036 (2009). https://doi.org/10.1103/PhysRevD.80.024036
78. Y. Liu, S. Chen, J. Jing, Strong gravitational lensing in a squashed Kaluza–Klein black hole spacetime. Phys. Rev. D **81**, 124017 (2010). https://doi.org/10.1103/PhysRevD.81.124017
79. C. Ding et al., Strong gravitational lensing in a noncommutative black-hole spacetime. Phys. Rev. D **83**, 084005 (2011). https://doi.org/10.1103/PhysRevD.83.084005
80. H. Sotani, U. Miyamoto, Strong gravitational lensing by an electrically charged black hole in Eddington-inspired Born–Infeld gravity. Phys. Rev. D **92**, 044052 (2015). https://doi.org/10.1103/PhysRevD.92.044052

81. N. Tsukamoto, Affine perturbation series of the deflection angle of a ray near the photon sphere of a Reissner–Nordström black hole. Phys. Rev. D **106**, 084025 (2022). https://doi.org/10.1103/PhysRevD.106.084025
82. N. Tsukamoto, Gravitational Lensing by using the 0th order of affine perturbation series of the deflection angle of a ray near a photon sphere. EPJC **83**, 284 (2023). https://doi.org/10.1140/epjc/s10052-023-11419-9
83. A. Chowdhuri, S. Ghosh, A. Bhattacharyya, A review on analytical studies in gravitational lensing. Front. Phys. **11**, 1113909 (2023). https://doi.org/10.3389/fphy.2023.1113909
84. A.R. Soares et al., Holonomy corrected Schwarzschild black hole lensing. Phys. Rev. D **108**, 124024 (2023). https://doi.org/10.1103/PhysRevD.108.124024
85. G. Mustafa, S.K. Maurya, Testing strong gravitational lensing effects of various supermassive compact objects for the static and spherically symmetric hairy black hole by gravitational decoupling. EPJC **84**, 686 (2024). https://doi.org/10.1140/epjc/s10052-024-13057-1
86. X.M. Kuang et al., Constraining a modified gravity theory in strong gravitational lensing and black hole shadow observations. Phys. Rev. D **106**, 064012 (2022). https://doi.org/10.1103/PhysRevD.106.064012
87. K.S. Virbhadra, G.F.R. Ellis, Schwarzschild black hole lensing. Phys. Rev. D **62**, 084003 (2000). https://doi.org/10.1103/PhysRevD.62.084003
88. K.S. Virbhadra, Relativistic images of Schwarzschild black hole lensing. Phys. Rev. D **79**, 083004 (2009). https://doi.org/10.1103/PhysRevD.79.083004
89. K.S. Virbhadra, Distortions of images of Schwarzschild lensing. Phys. Rev. D **106**, 064038 (2022). https://doi.org/10.1103/PhysRevD.106.064038
90. K.S. Virbhadra, Conservation of distortion of gravitationally lensed images. Phys. Rev. D **109**, 124004 (2024). https://doi.org/10.1103/PhysRevD.109.124004
91. K.S. Virbhadra, G.F.R. Ellis, Gravitational lensing by naked singularities. Phys. Rev. D **65**, 103004 (2002). https://doi.org/10.1103/PhysRevD.65.103004
92. V. Bozza, L. Mancini, Time delay in black hole gravitational lensing as a distance estimator. Gen. Relativ. Gravit. **36**, 435 (2004). https://doi.org/10.1023/B:GERG.0000010486.58026.4f
93. T. Hsieh, D.S. Lee, C.Y. Lin, Gravitational time delay effects by Kerr and Kerr–Newman black holes in strong field limits. Phys. Rev. D **104**, 104013 (2021). https://doi.org/10.1103/PhysRevD.104.104013
94. S.U. Islam, J. Kumar, S.G. Ghosh, Strong gravitational lensing by rotating Simpson–Visser black holes. J. Cosmol. Astropart. Phys. **2021**, 013 (2021). https://doi.org/10.1088/1475-7516/2021/10/013
95. R.T. Cavalcanti, A.G. Da Silva, R. Da Rocha, Strong deflection limit lensing effects in the minimal geometric deformation and Casadio–Fabbri–Mazzacurati solutions. Class. Quantum Gravity **33**, 215007 (2016). https://doi.org/10.1088/0264-9381/33/21/215007
96. X. Lu, F.W. Yang, Y. Xie, Strong gravitational field time delay for photons coupled to Weyl tensor in a Schwarzschild black hole. EPJC **76**, 357 (2016). https://doi.org/10.1140/epjc/s10052-016-4218-2
97. E.F. Eiroa, C.M. Sendra, Regular phantom black hole gravitational lensing. Phys. Rev. D **88**, 103007 (2013). https://doi.org/10.1103/PhysRevD.88.103007
98. T. Zhu et al., Shadows and deflection angle of charged and slowly rotating black holes in Einstein-Æther theory. Phys. Rev. D **100**, 044055 (2019). https://doi.org/10.1103/PhysRevD.100.044055
99. G.W. Gibbons, M.C. Werner, Applications of the Gauss–Bonnet theorem to gravitational lensing. Class. Quantum Gravity **25**, 235009 (2008). https://doi.org/10.1088/0264-9381/25/23/235009
100. M.P. Do Carmo, Differential Geometry of Curves and Surfaces (Dover Publications, Mineola, New York, 2016). https://books.google.com/books?hl=en&lr=&id=gg2xDQAAQBAJ&oi=fnd&pg=PR11&ots=waHmx0PO4G&sig=7UBN6dtL9oVb4FZfuCFNblkOqJ4
101. W. Klingenberg, *A Course in Differential Geometry* (Springer, New York, 1978). https://books.google.com/books?hl=en&lr=&id=usoFCAAAQBAJ&oi=fnd&pg=PA1&ots=1YZ8mpkXtH&sig=scxgjeAIav8qkIUwm0gzP1rF9hw
102. K. Jusufi et al., Light deflection by a rotating global monopole spacetime. Phys. Rev. D **95**, 104012 (2017). https://doi.org/10.1103/PhysRevD.95.104012
103. I. Sakalli, A. Övgün, Hawking radiation and deflection of light from Rindler modified Schwarzschild black hole. EPL **118**, 60006 (2017). https://doi.org/10.1209/0295-5075/118/60006
104. A. Övgün, Weak field deflection angle by regular black holes with cosmic strings using the Gauss–Bonnet theorem. Phys. Rev. D **99**, 104075 (2019). https://doi.org/10.1103/PhysRevD.99.104075
105. A. Övgün, G. Gyulchev, K. Jusufi, Weak gravitational lensing by phantom black holes and phantom wormholes using the Gauss–Bonnet theorem. Ann. Phys. **406**, 152 (2019). https://doi.org/10.1016/j.aop.2019.04.007
106. R. Kumar, S.G. Ghosh, A. Wang, Gravitational deflection of light and shadow cast by rotating Kalb–Ramond black holes. Phys. Rev. D **101**, 104001 (2020). https://doi.org/10.1103/PhysRevD.101.104001
107. Y. Pahlavon et al., Effect of magnetized plasma on shadow and gravitational lensing of a Reissner–Nordström black hole. Phys. Dark Univ. **45**, 101543 (2024). https://doi.org/10.1016/j.dark.2024.101543
108. Z. Li, A. Övgün, Finite-distance gravitational deflection of massive particles by a Kerr-like black hole in the bumblebee gravity model. Phys. Rev. D **101**, 024040 (2020). https://doi.org/10.1103/PhysRevD.101.024040
109. S.K. Jha, A. Rahaman, Strong gravitational lensing in Hairy Schwarzschild background. Eur. Phys. J. Plus **138**, 86 (2023). https://doi.org/10.1140/epjp/s13360-023-03650-w
110. B. Eslam Panah, K. Jafarzade, S.H. Hendi, Charged 4D Einstein–Gauss–Bonnet-AdS black holes: shadow, energy emission, deflection angle and heat engine. Nucl. Phys. B **961**, 115269 (2020). https://doi.org/10.1016/j.nuclphysb.2020.115269
111. C.K. Qiao, M. Zhou, The gravitational bending of acoustic Schwarzschild black hole. EPJC **83**, 271 (2023). https://doi.org/10.1140/epjc/s10052-023-11376-3
112. M.C. Werner, Gravitational lensing in the Kerr–Randers optical geometry. Gen. Relativ. Gravit. **44**, 3047 (2012). https://doi.org/10.1007/s10714-012-1458-9
113. K. Jusufi et al., Deflection of light by rotating regular black holes using the Gauss–Bonnet theorem. Phys. Rev. D **97**, 124024 (2018). https://doi.org/10.1103/PhysRevD.97.124024
114. A. Ishihara et al., Gravitational bending angle of light for finite distance and the Gauss–Bonnet theorem. Phys. Rev. D **94**, 084015 (2016). https://doi.org/10.1103/PhysRevD.94.084015
115. T. Ono, A. Ishihara, H. Asada, Gravitomagnetic bending angle of light with finite-distance corrections in stationary axisymmetric spacetimes. Phys. Rev. D **96**, 104037 (2017). https://doi.org/10.1103/PhysRevD.96.104037
116. R. Kumar, S.G. Ghosh, A. Wang, Shadow cast and deflection of light by charged rotating regular black holes. Phys. Rev. D **100**, 124024 (2019). https://doi.org/10.1103/PhysRevD.100.124024
117. G. Crisnejo, E. Gallo, K. Jusufi, Higher order corrections to deflection angle of massive particles and light rays in plasma media for stationary spacetimes using the Gauss–Bonnet theorem. Phys.

Rev. D **100**, 104045 (2019). https://doi.org/10.1103/PhysRevD.100.104045
118. T. Ono, H. Asada, The effects of finite distance on the gravitational deflection angle of light. Universe **5**, 218 (2019). https://doi.org/10.3390/universe5110218
119. S. Panpanich, S. Ponglertsakul, L. Tannukij, Particle motions and gravitational lensing in de Rham–Gabadadze–Tolley massive gravity theory. Phys. Rev. D **100**, 044031 (2019). https://doi.org/10.1103/PhysRevD.100.044031
120. K. Takizawa, T. Ono, H. Asada, Gravitational deflection angle of light: definition by an observer and its application to an asymptotically nonflat spacetime. Phys. Rev. D **101**, 104032 (2020). https://doi.org/10.1103/PhysRevD.101.104032
121. Í.D.D. Carvalho et al., The gravitational bending angle by static and spherically symmetric black holes in bumblebee gravity. EPL **134**, 51001 (2021). https://doi.org/10.1209/0295-5075/134/51001
122. F. Atamurotov, S.G. Ghosh, Gravitational weak lensing by a naked singularity in plasma. Eur. Phys. J. Plus **137**, 662 (2022). https://doi.org/10.1140/epjp/s13360-022-02885-3
123. Y. Chen et al., Gravitational lensing by Born–Infeld naked singularities. Phys. Rev. D **109**, 084014 (2024). https://doi.org/10.1103/PhysRevD.109.084014
124. M.K. Hossain et al., Gravitational deflection of massive body around naked singularity. Nucl. Phys. B **1005**, 116598 (2024). https://doi.org/10.1016/j.nuclphysb.2024.116598
125. R. Shaikh et al., Strong gravitational lensing by wormholes. JCAP **2019**, 028 (2019). https://doi.org/10.1088/1475-7516/2019/07/028
126. S. Kumar, A. Uniyal, S. Chakrabarti, Shadow and weak gravitational lensing of rotating traversable wormhole in nonhomogeneous plasma spacetime. Phys. Rev. D **109**, 104012 (2024). https://doi.org/10.1103/PhysRevD.109.104012
127. N. Godani, G.C. Samanta, Gravitational lensing for wormhole with scalar field in f(R) gravity. IJGMMP **20**, 2350075 (2023). https://doi.org/10.1142/S0219887823500755
128. S. Kalita, S. Bhatporia, A. Weltman, Gravitational lensing in modified gravity: a case study for fast radio bursts. J. Cosmol. Astropart. Phys. **2023**, 059 (2023). https://doi.org/10.1088/1475-7516/2023/11/059
129. F.B. Davies et al., Constraining the gravitational lensing of $z \geq 6$ quasars from their proximity zones. ApJL **904**, L32 (2020). https://doi.org/10.3847/2041-8213/abc61f
130. R.C. Pantig, A. Övgün, Dark matter effect on the weak deflection angle by black holes at the Center of Milky Way and M87 Galaxies. EPJC **82**, 391 (2022). https://doi.org/10.1140/epjc/s10052-022-10319-8
131. W. Javed et al., Weak deflection angle by Kalb–Ramond traversable wormhole in plasma and dark matter mediums. Universe **8**, 599 (2022). https://doi.org/10.3390/universe8110599
132. R. Karmakar, U.D. Goswami, Quasinormal modes, thermodynamics and shadow of black holes in Hu–Sawicki f(R) gravity theory. EPJC **84**, 969 (2024). https://doi.org/10.1140/epjc/s10052-024-13359-4
133. J.F. Donoghue, G. Menezes, The Ostrogradsky instability can be overcome by quantum physics. Phys. Rev. D **104**, 045010 (2021). https://doi.org/10.1103/PhysRevD.104.045010
134. Tai-jun Chen et al., Higher derivative theories with constraints: exorcising Ostrogradski's ghost. JCAP **1302**, 042 (2013). https://doi.org/10.1088/1475-7516/2013/02/042
135. M. Martinelli, A. Melchiorri, L. Amendola, Cosmological constraints on the Hu–Sawicki modified gravity scenario. Phys. Rev. D **79**, 123516 (2009). https://doi.org/10.1103/PhysRevD.79.123516
136. R.T. Hough, A. Abebe, S.E.S. Ferreira, Viability tests of f(R)-gravity models with supernovae type 1A data. EPJC **80**, 787 (2020). https://doi.org/10.1140/epjc/s10052-020-8342-7
137. J.B. Orjuela-Quintana, S. Nesseris, Tracking the validity of the quasi-static and sub-horizon approximations in modified gravity. JCAP **2023**, 019 (2023). https://doi.org/10.1088/1475-7516/2023/08/019
138. R. Kou, C. Murray, J.G. Bartlett, Constraining f(R) gravity with cross-correlation of galaxies and cosmic microwave background lensing. A&A **686**, A193 (2024). https://doi.org/10.1051/0004-6361/202348639
139. S. Fakhry, M. Shiravand, M. Farhang, Primordial black hole-neutron star merger rate in modified gravity. ApJ **966**, 235 (2024). https://doi.org/10.3847/1538-4357/ad3a66
140. S. Lyall, C. Blake, R.J. Turner, Constraining modified gravity scenarios with the 6dFGS and SDSS Galaxy peculiar velocity data sets. Mon. Not. R. Astron. Soc. **532**, 3972 (2024). https://doi.org/10.1093/mnras/stae1718
141. B. Santos et al., Cosmology with Hu–Sawicki gravity in the Palatini formalism. A&A **548**, A31 (2019). https://doi.org/10.1051/0004-6361/201220278
142. R. Kumar et al., Investigating the accelerated expansion of the Universe through updated constraints on viable f(R) models within the metric formalism. Mnras **527**, 7626 (2024). https://doi.org/10.1093/mnras/stad3705
143. A.D. Felice, S. Tsujikawa, f(R) theories. Liv. Rev. Relativ. **13**, 3 (2010). https://doi.org/10.12942/lrr-2010-3
144. S. Chakraborty, S. Chakraborty, Does the stability of f(R) theories imply the stability of the dual scalar-tensor theory?. (2024). https://doi.org/10.48550/arXiv.2411.09992. arXiv:2411.09992
145. F. Kottler, Über die physikalischen Grundlagen der Einsteinschen Gravitations theorie. Ann. Phys. **361**, 401 (1918). https://doi.org/10.1002/andp.19183611402
146. K. Nakashi et al., Null geodesics and repulsive behavior of gravity in $(2+1)$D massive gravity. Prog. Theor. Exp. Phys. (2019). https://doi.org/10.1093/ptep/ptz062
147. T. Kitamura, K. Nakajima, H. Asada, Demagnifying gravitational lenses toward hunting a clue of exotic matter and energy. Phys. Rev. D **87**, 027501 (2013). https://doi.org/10.1103/PhysRevD.87.027501
148. S. Weinberg, *Gravitation and Cosmology: Principles and Applications of the General Theory of Relativity* (Wiley, New York, 1972)
149. N. Tsukamotoand, Deflection angle in the strong deflection limit in a general asymptotically flat, static, spherically symmetric spacetime. Phys. Rev. D **95**, 064035 (2017). https://doi.org/10.1103/PhysRevD.95.064035
150. K. Sarkar, A. Bhadra, Strong field gravitational lensing in scalar-tensor theories. Class. Quantum Gravity **23**, 6101 (2006). https://doi.org/10.1088/0264-9381/23/22/002
151. J.S.U. Islam, S.G. Ghosh, Strong gravitational lensing by loop quantum gravity motivated rotating black holes and EHT observations. EPJC **83**, 1014 (2023). https://doi.org/10.1140/epjc/s10052-023-12205-3
152. S.U. Islam, S.G. Ghosh, S.D. Maharaj, Strong gravitational lensing by Bardeen black holes in 4D EGB gravity: constraints from supermassive black holes. Chin. J. Phys. **89**, 1710 (2024). https://doi.org/10.1016/j.cjph.2024.03.044
153. S.U. Islam, R. Kumar, S.G. Ghosh, Gravitational lensing by black holes in the 4D Einstein–Gauss–Bonnet gravity. JCAP **09**, 030 (2020). https://doi.org/10.1088/1475-7516/2020/09/030
154. J. Kumar, S.U. Islam, S.G. Ghosh, Investigating strong gravitational lensing effects by supermassive black holes with Horndeski gravity. EPJC **82**, 443 (2022). https://doi.org/10.1140/epjc/s10052-022-10357-2

155. E.F. Eiroa, C.M. Sendra, Gravitational lensing by a regular black hole. Class. Quantum Gravity **28**, 085008 (2011). https://doi.org/10.1088/0264-9381/28/8/085008
156. X.J. Gao et al., Investigating strong gravitational lensing with black hole metrics modified with an additional term. Phys. Lett. B **822**, 136683 (2021). https://doi.org/10.1016/j.physletb.2021.136683
157. N. Tsukamotoand, Gravitational lensing in the Simpson–Visser black-bounce spacetime in a strong deflection limit. Phys. Rev. D **103**, 024033 (2021). https://doi.org/10.1103/PhysRevD.103.024033
158. V. Bozza, S. Capozziello, G. Iovane, G. Scarpetta, Strong field limit of black hole gravitational lensing. Gen. Relativ. Gravit. **33**, 1535 (2001). https://doi.org/10.1023/A:3A1012292927358
159. A.M. Ghez et al., Measuring distance and properties of the Milky Way's central supermassive black hole with stellar orbits. APJ **689**, 1044 (2008). https://doi.org/10.1086/592738
160. S. Gillessen et al., Monitoring stellar orbits around the massive black hole in the galactic center. APJ **692**, 1075 (2009). https://doi.org/10.1088/0004-637X/692/2/1075
161. T. Do et al., Unprecedented near-infrared brightness and variability of $SgrA^*$. APJL **882**, L27 (2019). https://doi.org/10.3847/2041-8213/ab38c3
162. V. Bozza, Gravitational lensing by black holes. Gen. Relativ. Gravit. **42**, 2269 (2010). https://doi.org/10.1007/s10714-010-0988-2